

UC San Diego

UC San Diego Electronic Theses and Dissertations

Title

Electrochemical Polymerization as a Tool for Scalable Deposition of Polythiophene as the Hole-Transporting Layer in Perovskite Solar Cells

Permalink

<https://escholarship.org/uc/item/35s0n3sh>

Author

Fjeldberg, Oeystein

Publication Date

2019

Supplemental Material

<https://escholarship.org/uc/item/35s0n3sh#supplemental>

Peer reviewed|Thesis/dissertation

UNIVERSITY OF CALIFORNIA SAN DIEGO

Electrochemical Polymerization as a Tool for Scalable Deposition of
Polythiophene as the Hole-Transporting Layer in Perovskite Solar Cells

A Thesis submitted in partial satisfaction of the requirements for the degree
Master of Science

in

NanoEngineering

by

Oeystein Fjeldberg

Committee in charge:

Professor Ying Shirley Meng, Chair
Professor David Fenning
Professor Darren Lipomi

2019

The Thesis of Oeystein Fjeldberg is approved, and it is acceptable in quality and form for publication on microfilm and electronically:

Chair

University of California San Diego

2019

TABLE OF CONTENTS

Signature Page.....	iii
Table of Contents.....	iv
List of Abbreviations.....	vii
List of Supplemental Files.....	ix
List of Figures.....	x
List of Tables.....	xiii
Acknowledgments.....	xiv
Vita.....	xvi
Abstract of the Thesis.....	xvii
Chapter 1. Introduction: The Need for a Scalable Deposition Technique of the Hole-Transporting Layer in Perovskite Solar Cells.....	1
Chapter 2. Polythiophene Electrodeposition.....	5
2.1 Preliminary synthesis and characterization.....	5
2.1.1 Synthesis: Monitoring Growth by Cyclic Voltammetry.....	8
2.1.2 Confirming molecular identity by SEM-EDX and FTIR.....	10
2.2 Establishing electrochemical parameters.....	12
2.2.1 Electrochemical Cell Design.....	13
2.2.2 Electrolyte composition.....	15
2.2.2.1 Choice of Building Block.....	15
2.2.2.2 Concentration.....	18
2.2.3 Electrochemical biasing sequence.....	20
2.3 Large-Area Deposition.....	23
2.4 Summary.....	25

Chapter 3. Solar cells.....	26
3.1 Inverted Structure Solar Cells.....	27
3.1.1 Photoluminescence.....	28
3.1.2 Implementation into Solar Cells.....	30
3.1.3 Imaging of Polythiophene/Perovskite Interface by SEM.....	32
3.1.4 Economic Analysis.....	34
3.1.4.1 Material Costs.....	35
3.1.4.2 Capital and Operational Costs.....	37
3.1.4.3 Total Manufacturing Cost.....	40
3.1.5 Future Promise and Critical Analysis.....	41
3.2 Normal Structure Solar Cells.....	43
3.2.1 Designing Electrolytes with Low Polymerization Potentials....	44
3.2.2 Chemical stability tests.....	47
3.2.3 Electrochemical stability tests.....	49
3.2.3.1 Identifying Corrosion Events by Cyclic Voltammetry	50
3.2.3.2 Potentiostatic and Galvanostatic Studies.....	52
3.2.4 Conclusion.....	55
Chapter 4. Summary of the Thesis and Future Work.....	56
Chapter 5. Experimental setup.....	57
5.1 Electrodes.....	57
5.2 Electrochemical cell setup.....	57
5.2.1 Simple glass cell.....	57
5.2.2 PTFE cell.....	58
5.3 Electrolytes.....	59
5.4 Potentiostat.....	59
5.5 Synthesis, Wash, and Storage of Polythiophene films.....	59
5.6 Synthesis of thin film perovskites.....	59
5.6.1 $\text{CH}_3\text{NH}_3\text{PbI}_3$ (MAPbI ₃) perovskites.....	59
5.6.2 $\text{Cs}_{0.05}\text{FA}_{0.79}\text{MA}_{0.16}\text{Pb}(\text{Br}_{0.16}\text{I}_{0.84})_3$ (mixed-cation) perovskite....	60
5.7 Chemical and Electrochemical Stability Tests of Perovskite.....	60
5.8 Scanning electron microscopy (SEM).....	60
5.9 Fourier-Transform Infrared (FTIR) Spectroscopy.....	61
5.10 X-ray Diffraction (XRD).....	61
5.11 Ultraviolet - Visible (UV-Vis) Spectroscopy.....	61

5.12 Steady-state Photoluminescence (ss-PL)	61
5.13 Solar simulator	61
Bibliography	62

LIST OF ABBREVIATIONS

PSC	Perovskite Solar Cell
MAPbI ₃	Methylammonium lead iodide (CH ₃ NH ₃ PbI ₃) perovskite
CV	Cyclic Voltammetry
XRD	X-Ray Diffraction
SEM	Scanning Electron Microscope
WE	Working Electrode
CE	Counter Electrode
RE	Reference Electrode
EDX	Energy Dispersive X-Ray Spectroscopy
PCE	Photovoltaic Conversion Efficiency
J _{sc}	Short-circuit current density
V _{oc}	Open-circuit voltage (in the context of photovoltaic parameters)
FF	Fill Factor
R _{series}	Series resistance
R _{shunt}	Shunt resistance
ITO	Indium tin oxide
Spiro-OMeTAD	2,2',7,7'-tetrakis(N,N-di-pmethoxyphenyl-amine)9,9'-spirobifluorene
P3HT	Poly(3-hexylthiophene)
PEDOT	Poly(3,4-ethylenedioxythiophene)

PTAA	Poly(triarylamine)
PCBM	Phenyl-C ₆₁ -butyric acid methyl ester
JV	Current density – voltage
ss-PL	Steady-state photoluminescence
Bu ₄ NPF ₆	Tetrabutylammonium hexafluorophosphate
DCM	Dichloromethane
FTIR	Fourier-Transform Infrared Spectroscopy
UV-Vis	Ultraviolet-Visible

LIST OF SUPPLEMENTAL FILES

Supplemental File 1. Video of polymerization by cyclic voltammetry,
Fjeldberg_Video_of_polymerization_by_cyclic_voltammetry.mov

LIST OF FIGURES

Figure 1. Cost breakdown of a perovskite solar cell ^[2] . (a) Total manufacturing cost. (b) Material cost only	3
Figure 2. Molecular structure of polythiophene.....	4
Figure 3. Reaction mechanism for polymerization of thiophene.....	7
Figure 4. Reaction mechanisms at each electrode and in solution bulk during polymerization and doping.....	8
Figure 5. Voltammogram from polymerization in 10 mM 2,2'-bithiophene electrolyte for (a) the first cycle and (b) the second through sixth cycles.....	9
Figure 6. Molecular structure and photo of polythiophene in undoped and doped form.....	10
Figure 7. SEM-EDX spectrum of polythiophene film on ITO.....	11
Figure 8. FTIR spectrum of polythiophene film.....	11
Figure 9. Effect of counter electrode geometry on film deposition; photos of synthesized films and electric field lines for each WE-CE configuration.....	13
Figure 10. Schematics of electrode configurations as seen from above and photos of (a) simple glass cell and (b) PTFE cell.....	14
Figure 11. Cross-section SEM image of polythiophene films prepared in electrolyte containing 10 mM of a) thiophene dimer (2,2'-bithiophene) and b) thiophene trimer (2,2':5',2''-terthiophene). Scale bar: 100 nm	17
Figure 12. XRD of polythiophene films grown in dimer and trimer electrolytes.....	18
Figure 13. Photos of films grown in (a) 10 mM 2,2'-bithiophene and 0.1 M Bu ₄ NPF ₆ in simple glass cell; (b) 10 mM 2,2'-bithiophene and 0.1 M Bu ₄ NPF ₆ in PTFE cell, and; (c) 1 mM 2,2'-bithiophene and 0.01 M Bu ₄ NPF ₆ in PTFE cell. Width of image: 2.5 cm.....	19
Figure 14. Photos of films synthesized in electrolytes of varying 2,2'-bithiophene and Bu ₄ NPF ₆ concentrations. Width of image: 2.5 cm.....	19
Figure 15. Polythiophene morphology before optimization.....	20

Figure 16. Cross-section SEM image of polythiophene films electropolymerized with different quantities of delivered charge during deposition. Scale bar: 200 nm.....	21
Figure 17. Cross-section SEM image of polythiophene films electropolymerized at different voltages vs Ag/Ag ⁺ until reaching 10 mC/cm ² . Scale bar: 100 nm	21
Figure 18. Polythiophene morphology for film synthesized with final parameters, i.e. constant current of 0.02 mA/cm ² until reaching 3 mC/cm ²	22
Figure 19. Polythiophene film deposition. (a,b,c) Electrochemical cell setup, before (a,b) and after (c) adding electrolyte. (d) 10 cm x 10 cm polythiophene film deposited on ITO.....	23
Figure 20. SEM imaging of 10x10cm ² polythiophene film. (a) Inspected regions. (b) Cross-section imaging. (c) Top-view imaging.....	25
Figure 21. The two main types of PSC architectures. TCO: Transparent Conducting Oxide (i.e. ITO in this work)	26
Figure 22. UV-Vis transmittance of polythiophene films of various thicknesses.....	28
Figure 23. Ss-PL measurements of MAPbI ₃ /polythiophene/ITO.....	30
Figure 24. Solar cell performance of inverted structure PSCs with polythiophene as the HTL. (a) JV curve and PV parameters of champion cell. (b) Histogram of PCE efficiencies.....	32
Figure 25. Possible current pathways for an excited charge in a PSC. Undesirable pathways (shunt current, i.e. recombination) are marked in red and the desired pathway (photovoltaic current) is marked in green. Pathways due to incomplete coverage of layers (e.g. from ETL to HTL due to the two layers coming in direct contact as a result of pinholes in perovskite film) or defects (e.g. as a result of poor interfacial contact) are not included.....	32
Figure 26. Cross-section SEM image of inverted structure PSC with electrodeposited polythiophene. Scale bar: 100 nm.....	33
Figure 27. Material cost for each component of electrolyte required to electrodeposit polythiophene. (a) Cost per mL for 1 mM 2,2'-bithiophene / 0.01 M Bu ₄ NPF ₆ / DCM electrolyte. (b) Cost per square meter for depositing polythiophene from 1 mM 2,2'-bithiophene / 0.01 M Bu ₄ NPF ₆ / DCM electrolyte,	

assuming the electrolyte is discarded after a single deposition. (c) Cost per square meter for depositing polythiophene, assuming 100% material utilization and cost-effective recycling of DCM.....37

Figure 28. Manufacturing cost of electrodeposited polythiophene as HTL.....41

Figure 29. (a) A typical example of the first anodic sweep of a cyclic voltammetry electropolymerization. (b) Methodology for how polymerization potential for a given electrolyte composition is found.....45

Figure 30. (a) First anodic sweep of CV scan in various electrolyte compositions. (b) Overview of polymerization potentials for various electrolyte compositions. Voltages referenced against Ag/Ag⁺.....47

Figure 31. XRD plots of perovskite films after chemical stability tests for (a) MAPbI₃ and (b) (Cs_{0.05}FA_{0.79}MA_{0.16})Pb(Br_{0.16}I_{0.84})₃.....49

Figure 32. CV scans with MAPbI₃ on ITO as the working electrode in dimer and trimer electrolytes.....51

Figure 33. XRD of MAPbI₃ after CV scans in dimer and trimer electrolytes.....52

Figure 34. (a) XRD plot of MAPbI₃ perovskite films after electrochemical stability tests in 100 mM dimer electrolyte, biased at a constant potential for 2 min. (b) Photo of MAPbI₃ perovskite film after 2 min of bias at +0.75 V vs Ag/Ag⁺53

Figure 35. XRD of MAPbI₃ after chemical and electrochemical tests in DCM...54

LIST OF TABLES

Table 1. Effect of various electrochemical parameters on film properties.....12

Table 2. Properties of thiophene oligomers relevant to their utility as building blocks in electrochemical polymerization.....16

ACKNOWLEDGMENTS

Ying Shirley Meng for giving me the opportunity to work in an environment with so many resources

Min-Cheol Kim for revitalizing my passion for photovoltaic research and for being an amazing mentor

Shen Wang for introducing me to the field of solar cell research and giving me useful pieces of advice that stuck with me through the remainder of my master program

David Fenning for many useful pieces of research advice during the CEC update meetings and for being a great teacher in my all-time favorite class, Nanoscale Solar Cell Engineering

The California Energy Commission for providing the funding that enabled this project, and for giving me the flexibility to focus on what I deemed most important for developing electrochemical polymerization as a scalable deposition technique

Xiaowei for sharing his expertise on electrochemical polymerizations. His guidance was what finally made me crack the code to achieving high reproducibility in my results, and probably saved me from many additional weeks of wasted efforts and stress.

Dan Davies for helping me design the electrochemical cell used in this work (the PTFE cell)

Moses Kodur for giving me hours of his time to help me prepare samples on many occasions. Thank you for working with me to re-establish the journal club as a more engaging venture, and for the many interesting discussions that helped me build a deeper understanding of the solar cell literature. Also, thank you for just being a fun person in general to work with

The rest of the good people in the Fenning group for always being generous and helpful in assisting me when I needed to perform spin-coating inside their glovebox, use their glass cutter, etc. Special thanks to Taewoo Kim for helping me set up my first ever electrochemical cell.

Jonathan Scharf for always believing in me, even when I didn't do it myself. Thank you for the many conversations, both the research-related ones, the personal ones, and the silly ones.

Macwin for always being there to listen when I needed it.

My parents, Geir Fjeldberg and Turid Helen Gangenes, for always being supportive.

VITA

- 2013-2017 Bachelor of Science in Chemistry, Wingate University, NC, USA
- 2018-2019 Graduate Student Researcher, University of California San Diego
- 2019 Teaching Assistant, University of California San Diego
- 2019 Master of Science, University of California San Diego

FIELDS OF STUDY

Major Field: Engineering

Studies in NanoEngineering with focus on Nanotechnologies for Energy and the Environment

Professor Ying Shirley Meng

ABSTRACT OF THE THESIS

Electrochemical Polymerization as a Tool for Scalable Deposition of
Polythiophene as the Hole-Transporting Layer in Perovskite Solar Cells

by

Oeystein Fjeldberg

Master of Science in NanoEngineering

University of California San Diego, 2019

Professor Ying Shirley Meng, Chair

Perovskite solar cells (PSCs) have only been around for ten years, but have already demonstrated photovoltaic conversion efficiencies (PCEs) approaching those of state-of-the-art silicon photovoltaics. One of the critical challenges remaining is to develop solar cell fabrication methods that are compatible with industrial-scale production. Although the cost of the perovskite layer itself is cheap, the device also requires a hole-transporting layer (HTL), which is usually made from prohibitively expensive materials. Additionally, the HTL is commonly deposited through spin-coating, which leads to non-uniform film thickness for large-area substrates. By using electrochemical polymerization to deposit polythiophene as part of the solar cell fabrication procedure, these two problems can be overcome, as it allows for uniform thickness of the deposited layer and utilizes cheap precursors. In this study, polythiophene films were grown and characterized by Scanning Electron Microscopy (SEM) imaging to gain an understanding of how growth conditions affect film morphology and uniformity. Characterizations by Cyclic Voltammetry (CV), Fourier Transform Infrared Spectroscopy (FTIR), Energy-Dispersive X-Ray Spectroscopy (EDX), and X-Ray Diffraction (XRD) were also performed. Based on these results, I developed a method for large-area deposition that is compatible with industrial-scale solar cell production. This method was used to fabricate inverted structure PSCs with polythiophene as the HTL. In situ electrochemical polymerization of polythiophene onto perovskite for use in normal structure PSCs was also explored.

Chapter 1. Introduction: The Need for a Scalable Deposition Technique of the Hole-Transporting Layer in Perovskite Solar Cells

Perovskite solar cells (PSCs) have improved rapidly in terms of performance in the last decade, reaching efficiencies approaching those of state-of-the-art silicon photovoltaic research cells^[1]. Among the major bottlenecks currently prohibiting industrial implementation are high material costs (shown in Figure 1a) and a lack of scalable manufacturing methods for the active layers of the cell.

The perovskite material itself is cheap, making up $\sim \$1/\text{m}^2$ of the cost in solar cells^[2], but PSCs also require charge-transporting layers and current collectors. The charge-transporting layers, i.e., the electron-transporting layer (ETL) and the hole-transporting layer (HTL), create an asymmetry in the device that allows for the separation of negative and positive charges; the perovskite layer is sandwiched between the ETL and HTL, so that excited electrons are collected at the ETL interface and hole quasi-particles at the HTL interface. Current collectors are in contact with the ETL and HTL to draw the charges into the external circuit and harvest the energy. Unfortunately, materials with beneficial properties as HTLs in PSCs tend to be expensive, to the point where the HTL is the single greatest contributor to the overall cost of PSCs, as shown in Figure 1b.

Additionally, there is a need for a method of depositing the hole-transporting layer (HTL) that is compatible with large-area substrates. Spin-coating, which is

the standard deposition method in most PSC literature^[1], produces a layer of non-uniform thickness across large areas^[3]. What's more, the technique is wasteful, as >95% of the material is swept away from the substrate during the spinning process^[3], effectively scaling up the material cost >20 times. It has been estimated that, as a result of this low material utilization, spin-coated Spiro-OMeTAD (a popular high-performance HTL for PSCs) would have an effective material cost of \$200/m² ^[4]. Therefore, a deposition method should be developed that produces uniform films across large areas with low material costs.

Conducting polymers are often employed as the HTL in PSCs and are responsible for some of the highest reported efficiencies to date. Thiophene-based polymers are among the top performers, including poly(3-hexylthiophene) (P3HT) and poly(3,4-ethylenedioxythiophene) (PEDOT), which have demonstrated 22.7%^[5] and 18.7%^[6] photovoltaic conversion efficiencies (PCE), respectively. Unfortunately, both are expensive, with list prices at Sigma-Aldrich exceeding several hundred dollars per gram for photovoltaic-grade quality. Even if P3HT is deposited with a 95% material utilization rate, it still makes up a significant portion of the total PSC cost^[2], as shown in Figure 1b.

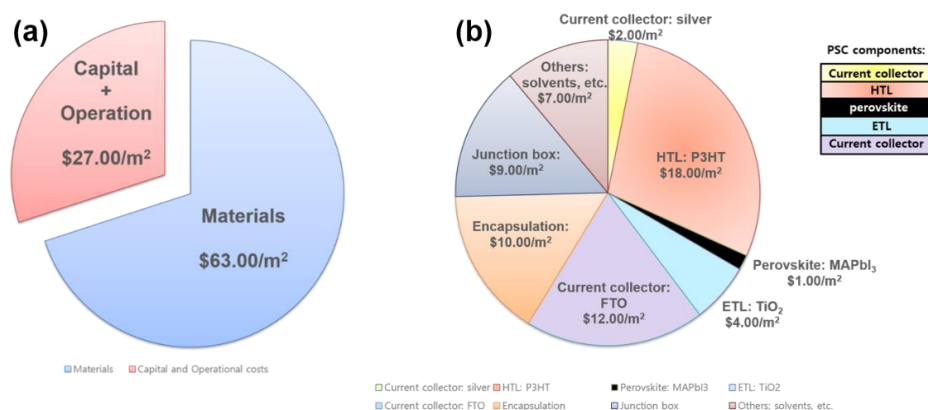


Figure 1. Cost breakdown of a perovskite solar cell^[2]. (a) Total manufacturing cost. (b) Material cost only

Yan et al. attempted to circumvent this issue by electrochemically polymerizing thiophene onto a transparent conducting electrode for use as the HTL in PSCs^[7]. In this way, polythiophene (Figure 2) could be generated from the extremely low-cost thiophene monomer (<0.01\$/g from Sigma-Aldrich), reducing the HTL material cost to a fraction of that of P3HT and other candidates. Furthermore, the electrochemical deposition technique allows for uniform film thickness over large areas^[8]. Nevertheless, their method involved the use of the highly toxic solvent boron trifluoride diethyl etherate (BFEE), introducing severe workplace hazards if implemented in industry, and was only applied to <1cm² substrates. Thus, electrochemical polymerization has yet to prove itself as a scalable deposition technique.

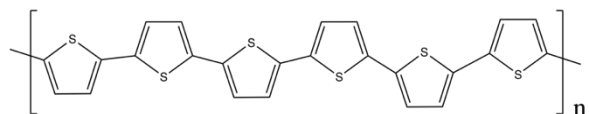


Figure 2. Molecular structure of polythiophene

In this thesis, I have developed experimental parameters for milliscale and nanoscale uniform deposition of polythiophene from cheap precursors over large areas (4-100 cm²). I have implemented the deposited films in inverted structure PSCs and investigated whether the method can be applied to normal structure PSCs as well.

Chapter 2. Polythiophene Electrodeposition

Electrochemical polymerization offers a facile way to prepare the hole-transporting layer for perovskite solar cells, as it can be synthesized from cheap materials and leads to the formation of a compact, uniform film.

Here, I began my studies by synthesizing polythiophene following experimental parameters from a previous report^[9], performed characterizations to verify its identity, established general electrochemical parameters for optimization of film uniformity, and applied the methodology to a large-area substrate. All films were deposited on indium tin oxide (ITO) working electrodes. All depositions were performed in ambient air to make the overall process better suited for industrial implementation; the risk of moisture participating in the electrochemical reactions was considered to be negligible due to the dichloromethane (DCM) electrolyte being immiscible with water, thus serving as a barrier to prevent water from entering the system.

2.1 Preliminary Synthesis and Characterization

Electrodeposition through polymerization differs from metal electrodeposition in that the active species in the reaction is not a cation that is reduced to a neutral state but rather a neutral organic molecule that is oxidized to form a positively charged radical, which then follows the free radical polymerization mechanism to form the polymer. Deposition occurs as a result of the polymer

growing to a chain length where it is no longer soluble in the solvent, causing it to precipitate as a film on the working electrode^[10].

The traditional polymerization mechanism to form polythiophene (shown in Figure 3) begins with the thiophene monomer^[11]. By applying a positive bias to a working electrode immersed in a thiophene solution, a single electron is removed from a thiophene ring near the electrode surface. The radicalized thiophene molecule then bonds with another thiophene radical and, upon elimination of the hydrogens to restore aromaticity of the molecule, the thiophene dimer, 2,2'-bithiophene, is formed. The dimer may then, in turn, become radicalized as well, continuing the growth of the chain, producing trimers, tetramers, etc. The polymerization thus follows the conventional free radical polymerization mechanism. Once the chains grow to a certain length, the attractive van der Waals forces between neighboring chains will overcome the solvation forces that kept them separated before, and the polymer will deposit as a compact film on the working electrode. Thus, the deposition depends on a supersaturation near the working electrode surface and will, as a result, not occur if stirring is used in the electrolyte. The polymerization will continue as long as 1) a positive overpotential is sustained at the working electrode, and 2) there is a non-zero surface concentration of thiophene at the working electrode.

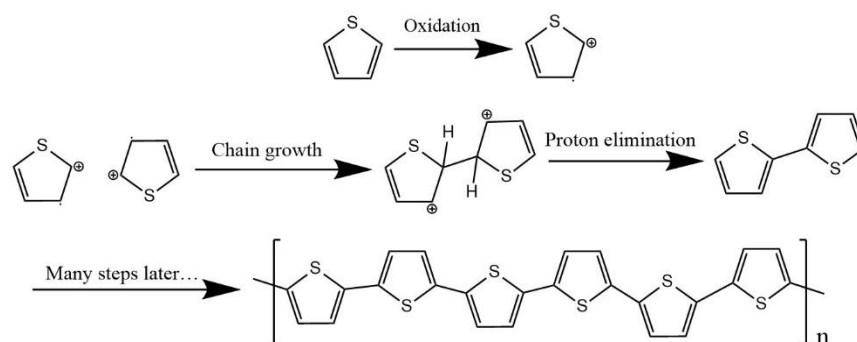


Figure 3. Reaction mechanism for polymerization of thiophene

Polythiophene is interesting as a semiconductor material because, among other characteristics, it can be reversibly doped, i.e., any doped polythiophene film can be made intrinsic, and vice versa^[12]. This can be done by simply immersing the film in an appropriate electrolyte and applying a positive or negative bias to dope or de-dope the film, respectively. Chemical doping and de-doping (i.e., without biasing) is also possible. During electrochemical doping, electrons are withdrawn from the film, generating positively charged hole quasi-particles along the polymer backbone (see Figure 4). Simultaneously, negatively charged ions from the electrolyte migrate through the film to preserve electroneutrality. The de-doping process is the reverse of this mechanism, i.e., electrons are pumped back into the film, and the anions are consequently expelled. The doping potential is usually lower than the polymerization potential, so doping will generally occur simultaneously with polymerization.

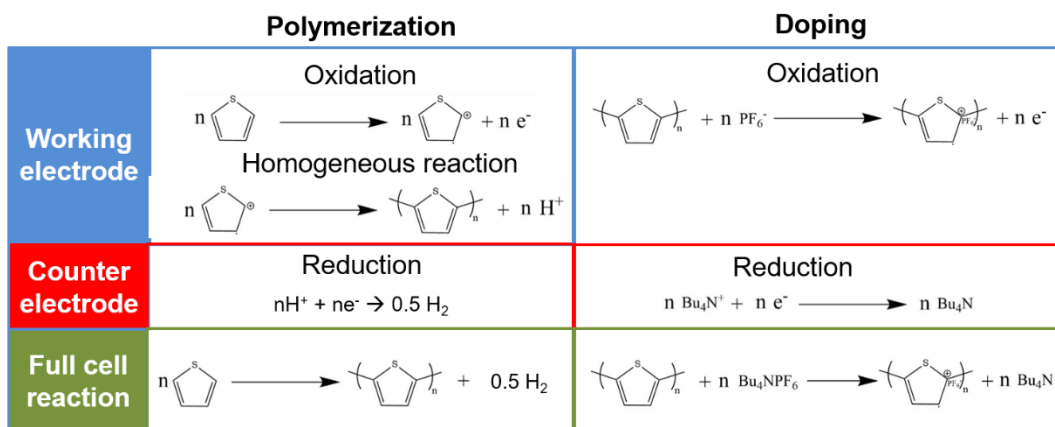


Figure 4. Reaction mechanisms at each electrode and in solution bulk during polymerization and doping

2.1.1 Synthesis: Monitoring Growth by Cyclic Voltammetry

In order to gain a preliminary understanding of the polymerization process, I initially grew polythiophene films on ITO in 10 mM 2,2'-bithiophene electrolyte with 0.1 M Bu_4NPF_6 in dichloromethane. Films were grown by cyclic voltammetry, which allowed me to monitor the growth of the film during deposition. In the first anodic sweep, there is a sharp current rise corresponding to polymerization (see Figure 5a). Simultaneously with the polymerization, negative ions from the electrolyte migrate into the polymer film, where they stabilize positive charges on the polymer backbone, doping the film. As the voltage is swept back in the cathodic direction, the negative ions are expelled from the film (de-doping), and this process appears as a broad peak centered at 0.31 V in the voltammogram. When the bias is scanned back towards positive voltages, a new redox peak appears prior to the polymerization onset (0.79 V); this peak corresponds to the re-doping

of the film. The integrated area of the re-doping and de-doping peaks ($Current\ density * Time = \frac{Charge\ delivered}{Area}$) serves as a rough indication of the quantity of film grown, as the amount of delivered charge correlates to the number of anions entering or exiting the film. Upon subsequent scans, the redox peaks corresponding to re-doping and de-doping of the film both grow in size (Figure 5b), indicating that the film is growing thicker and thus can hold onto a greater quantity of anions. As a result, the voltammogram retrieved from the CV scan may serve as a preliminary confirmation that the polymer was successfully synthesized^[13].

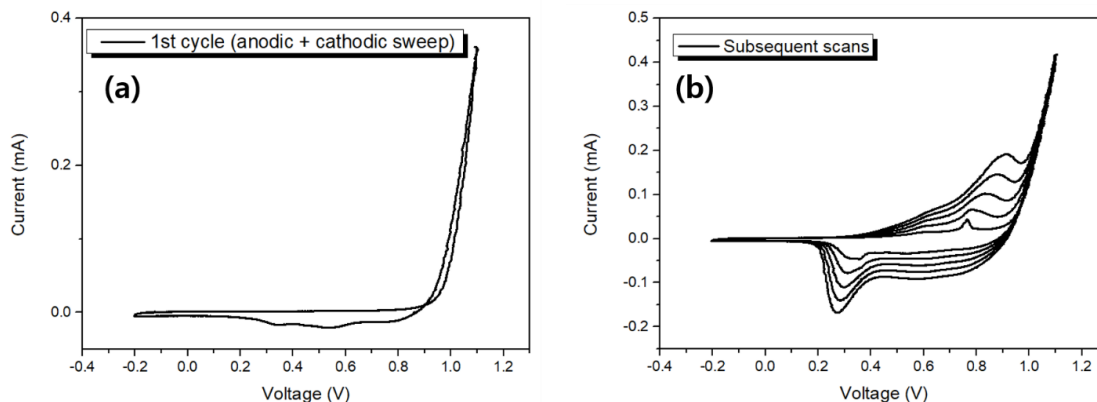


Figure 5. Voltammogram from polymerization in 10 mM 2,2'-bithiophene electrolyte for (a) the first cycle and (b) the second through sixth cycles

Growth by CV also offers the opportunity to observe one of the unique properties of polythiophene first-hand. The color of polythiophene depends on its doping level (as shown in Figure 6), so a repeated sequence back and forth between positive and negative bias will cause the film to alternate between red

(undoped) and blue (doped) color (demonstrated in Supplemental File 1). Since each anodic sweep leads to continued polymerization, the color will also become opaquer with each scan.

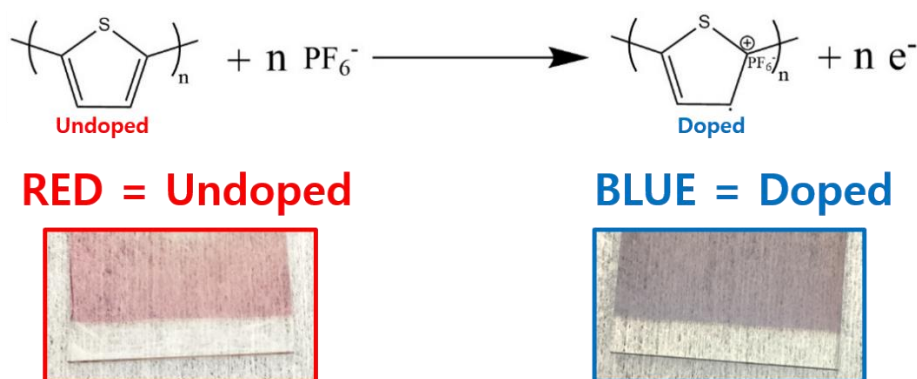


Figure 6. Molecular structure and photo of polythiophene in undoped and doped form

2.1.2 Confirming Molecular Identity by SEM-EDX and FTIR

After synthesis, the films were characterized by SEM-EDX and FTIR to verify whether a polythiophene film had been successfully produced.

EDX (Figure 7) revealed a peak at 2.30 keV, which is a unique characteristic of the K_{α} electronic transition in sulfur ($K_{\alpha}=2.307$ keV). The only other elements with a similar EDX characteristic energy are lead ($M=2.342$ keV) and molybdenum ($L_{\alpha}=2.293$ keV). Since neither lead nor molybdenum was present in the polymerization system, the peak could only be ascribed to the presence of sulfur in the film.

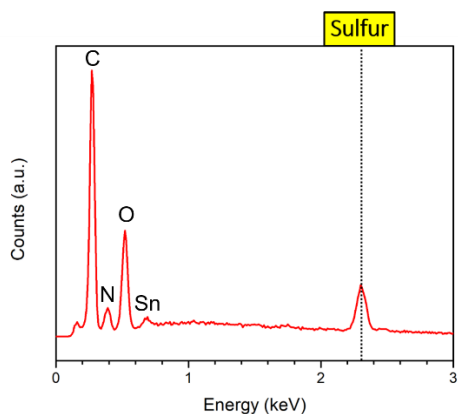


Figure 7. SEM-EDX spectrum of polythiophene film on ITO

Fourier-Transform Infrared (FTIR) spectroscopy (Figure 8) confirmed that polythiophene had been successfully synthesized, as the peaks for C-H stretching (3063cm^{-1}), C=C stretching (1491 cm^{-1} and 1440 cm^{-1}), and C-H bending (788 cm^{-1}) matched those of previously published results^[14].

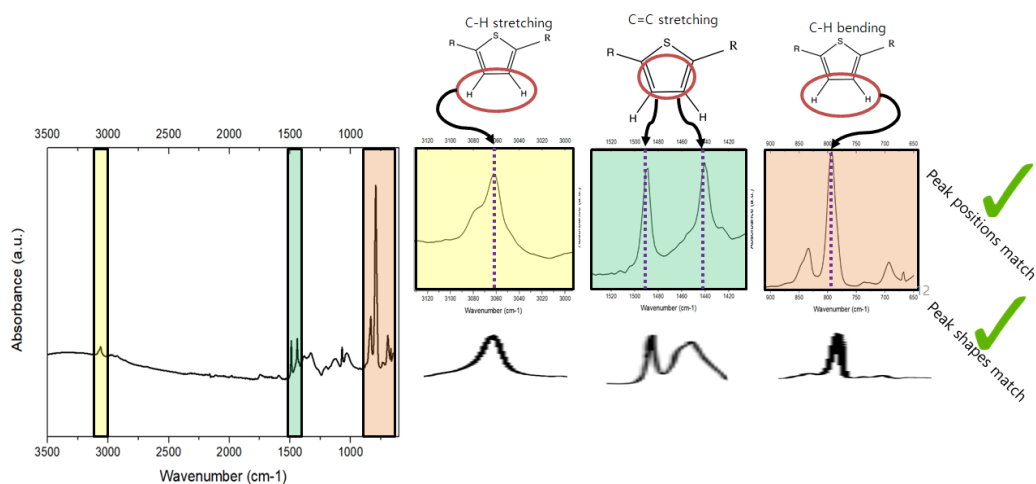






Figure 8. FTIR spectrum of polythiophene film

2.2 Establishing Electrochemical Parameters

In an electrochemical polymerization experiment, every experimental parameter has an impact on some aspect of the final film. Electrochemical cell design, electrolyte composition, and biasing sequence affects milliscale uniformity, material quality, and nanoscale uniformity, respectively^[15] (see Table 1). Temperature and the surrounding gas environment, although not investigated here, are also influential variables^[16]. For this section, I established guidelines for the optimization of the polythiophene growth process based on fundamental principles from electrochemistry and experimental results. The goal was to attain film uniformity on the milli- and nanoscale, as this was hypothesized to minimize inconsistencies in solar cell performance through the deposited film area, minimize surface recombination, and induce better crystallization of perovskite grains on polythiophene film. All experiments were performed with 2.5x2.5 cm² ITO as the working electrode.

Table 1. Effect of various electrochemical parameters on film properties

Experimental parameter	Factor(s)	Effect
Electrochemical cell design	Geometrical configuration of electrodes	 Uniformity: Milliscale
Electrolyte composition	Choice of thiophene oligomer	 Material quality
	Concentrations of thiophene oligomer and supporting electrolyte	 Uniformity: Milliscale
Electrochemical biasing sequence	Quantity of charge delivered	 Uniformity: Nanoscale
	Magnitude of overpotential	

2.2.1 Electrochemical Cell Design

The geometrical design of the electrochemical cell is critical to ensure milliscale uniformity. Previous electropolymerization methods have reported using a platinum wire as the counter electrode^[17], but this selection has limited utility for large-area working electrodes as the small surface area may limit its ability to compensate for charge build-up at high currents. To mitigate this, a counter electrode (CE) of equal or greater area than the working electrode (WE) should be used. Another concern is the geometrical configuration of the working and counter electrodes. The working electrode should be positioned parallel to the counter electrode, so that charge build-up is uniformly compensated throughout the working electrode surface, in turn leading to uniform film deposition (see Figure 9).

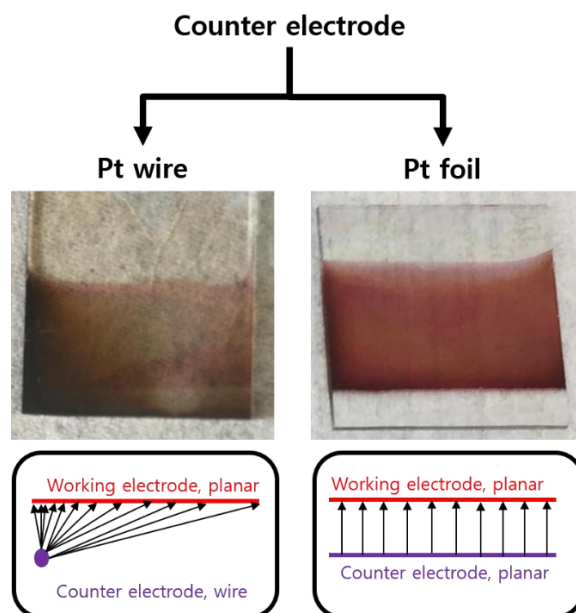


Figure 9. Effect of counter electrode geometry on film deposition; photos of synthesized films and electric field lines for each WE-CE configuration

Two electrochemical cell designs were used in this project (shown in Figure 10). Both were designed to maintain the WE and CE in parallel alignment at a fixed separation. The first setup, the simple glass cell, allowed for the synthesis of uniform films and was used for the preliminary experiments. The second setup, the PTFE cell, was developed to attain higher reproducibility (through more securely fixed WE and CE positions), reduce electrolyte usage (through the reduced volume container), and allow for constant current depositions (the WE exposed area was unknown in the simple glass cell).

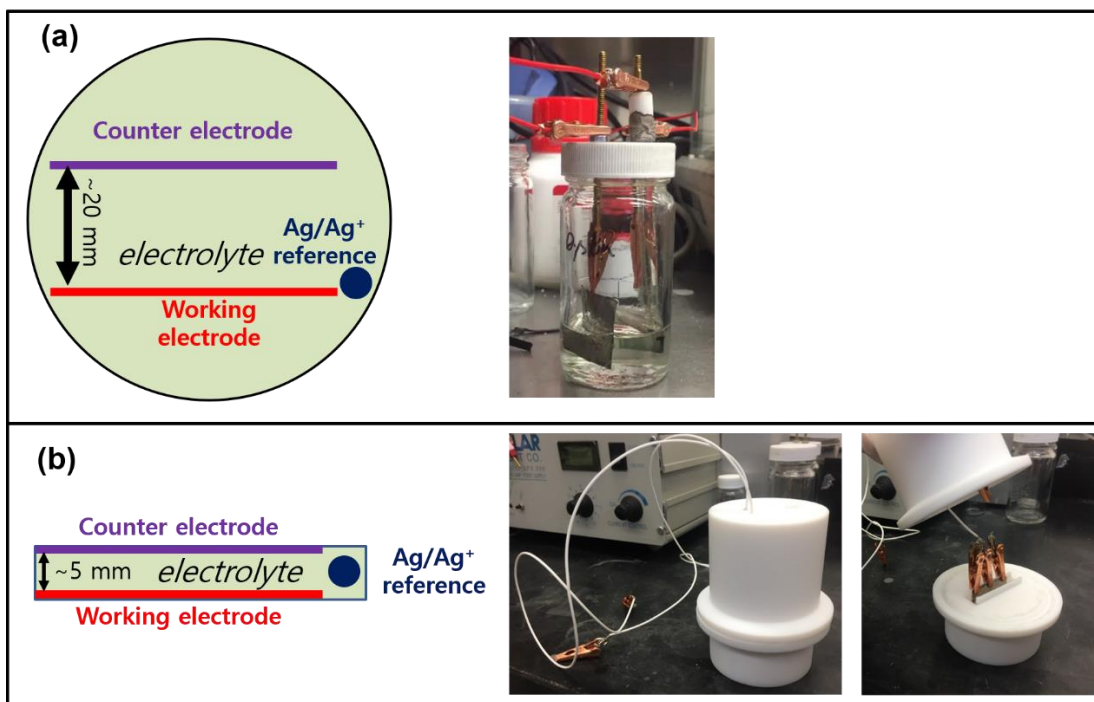


Figure 10. Schematics of electrode configurations as seen from above and photos of (a) simple glass cell and (b) PTFE cell

2.2.2 Electrolyte Composition

Electrolyte composition affects the material quality and morphology of the synthesized films. The choice of building block (i.e., monomer unit for polymerization), supporting electrolyte, and solvent all affect different aspects of the film morphology, as well as their respective concentrations^[15].

Dichloromethane (DCM) and tetrabutylammonium hexafluorophosphate (Bu_4NPF_6) were selected as solvent and supporting electrolyte because they are well-established in literature as a good solvent for polythiophenes and an electrochemically inert conducting agent^[18], respectively.

2.2.2.1 Choice of Building Block

One of the key challenges of polythiophene synthesis during the early stages of its discovery was that the voltage required to synthesize it simultaneously led to its degradation (nicknamed “The Polythiophene Paradox^[19]). In order to prevent polythiophene from degrading simultaneously with its synthesis, the polymerization potential must be brought below the degradation potential of polythiophene. This can be done by 1) substituting the thiophene monomer with a thiophene oligomer, which is easier to oxidize due to energy level splitting from reduced quantum confinement^[10], 2) increasing the thiophene concentration to shift the chemical equilibrium towards polythiophene formation, lowering the redox potential according to the Nernst equation^[10], or 3) using a Lewis acid such as

boron trifluoride ethyl etherate as the solvent, where the boron interacts with the pi electrons in the thiophene ring to shift their energy level upward^[10]. The third option was rejected because it requires the use of highly dangerous chemicals (e.g., boron trifluoride ethyl etherate, which reacts with the moisture in air to generate extremely toxic hydrogen fluoride gas). The first option (using an oligomer rather than the monomer of thiophene) was pursued because it offers the best compromise between material quality, price, and safety; the thiophene monomer is highly volatile and toxic, whereas the thiophene dimer and higher oligomers are all solids with low toxicity (see Table 2). Oligomers of thiophene tend to decrease in solubility with size, to the point where the hexamer, α -sexithiophene, has a solubility so low (0.25 g/L) that it is rendered unusable in electrodepositions^[20]. Therefore, the thiophene dimer (2,2'-bithiophene) and trimer (2,2':5',2''-terthiophene) were pursued as precursors because they retain a high solubility and low material cost.

Table 2. Properties of thiophene oligomers relevant to their utility as building blocks in electrochemical polymerization

	Polymerization potential in DCM (V vs Ag/AgCl) ^[20]	Solubility in DCM	Volatility	Toxicity	Price at Sigma-Aldrich (\$/g)
Monomer	1.55	High	High	High	0.098
Dimer	1.17	High	Low	Low	11
Trimer	0.96	High	Low	Low	121
Tetramer	0.90	No data	Low	No data	Not for sale
Pentamer	No data	No data	Low	No data	Not for sale
Hexamer	0.85	Low (0.25 g/L)	Low	Low	111

2,2'-bithiophene and 2,2':5',2''-terthiophene both fulfill the requirements of low polymerization potential, low cost, sufficient solubility, and low toxicity. In order to better understand which of the two oligomers offer the most promise as an HTL in PSCs, films were polymerized in electrolytes containing 10 mM dimer or trimer with 0.1 M Bu_4NPF_6 and brought to SEM for characterization. The quantity of delivered charge was 100 mC/cm^2 for the dimer and 67 mC/cm^2 for the trimer so that the total number of thiophene rings in the films were kept constant.

As can be seen in Figure 11, the film polymerized in dimer electrolyte exhibits far more dense morphology than the one polymerized in trimer electrolyte. XRD revealed a peak at 18.4° matching with literature reports for crystalline polythiophene^[21] for the film grown in dimer electrolyte (Figure 12), which was not present for the film grown with trimer building blocks, suggesting that polymerization from dimers led to a greater degree of film crystallinity. The exact reason for this phenomenon is not known. As a result of these tests, the thiophene dimer was selected as the building block for all subsequent polymerizations.

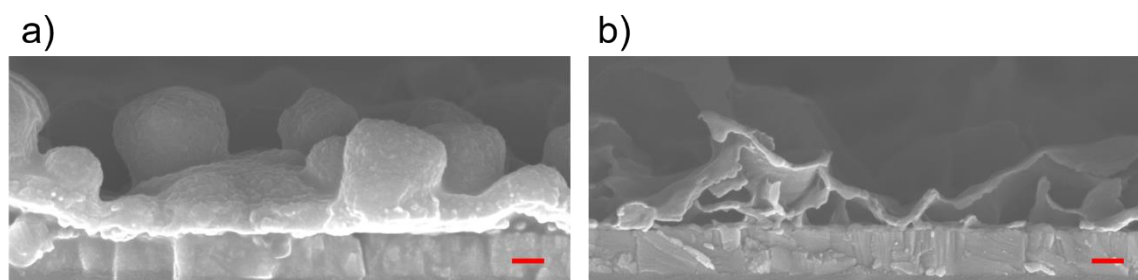


Figure 11. Cross-section SEM image of polythiophene films prepared in electrolyte containing 10 mM of a) thiophene dimer (2,2'-bithiophene) and b) thiophene trimer (2,2':5',2''-terthiophene). Scale bar: 100 nm

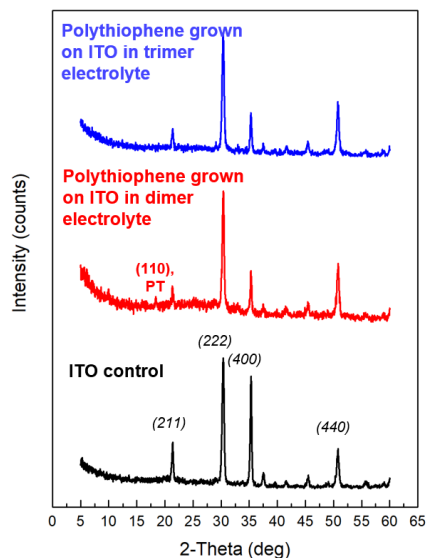


Figure 12. XRD of polythiophene films grown in dimer and trimer electrolytes

2.2.2.2 Concentration

Concentrations of 2,2'-bithiophene and Bu_4NPF_6 affected the milliscale uniformity of the deposited films to different degrees in the two different cell setups. The same electrolyte composition that allowed for uniform deposition in the simple glass cell setup (Figure 13a) (10 mM 2,2'-bithiophene and 0.1 M Bu_4NPF_6) led to spotty deposition in the PTFE cell setup (see Figure 13b). By utilizing an electrolyte with lower concentrations of 2,2'-bithiophene (from 10 mM to 1 mM) and Bu_4NPF_6 (from 0.1 M to 0.01 M), milliscale uniformity was restored (Figure 13c). In general, both 2,2'-bithiophene and Bu_4NPF_6 tended to allow for more uniform deposition at lower concentrations, as shown in Figure 14. The reason for the improved uniformity is not clear, but it may be an effect of the PTFE cell setup having a

narrower WE-CE gap than the simple glass cell setup (5 mm as opposed to 20 mm) or the reduced electrolyte volume (3.5 mL as opposed to 15 mL), or both.

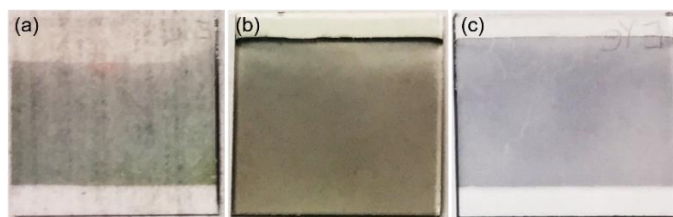


Figure 13. Photos of films grown in (a) 10 mM 2,2'-bithiophene and 0.1 M Bu_4NPF_6 in simple glass cell; (b) 10 mM 2,2'-bithiophene and 0.1 M Bu_4NPF_6 in PTFE cell, and; (c) 1 mM 2,2'-bithiophene and 0.01 M Bu_4NPF_6 in PTFE cell. Width of image: 2.5 cm

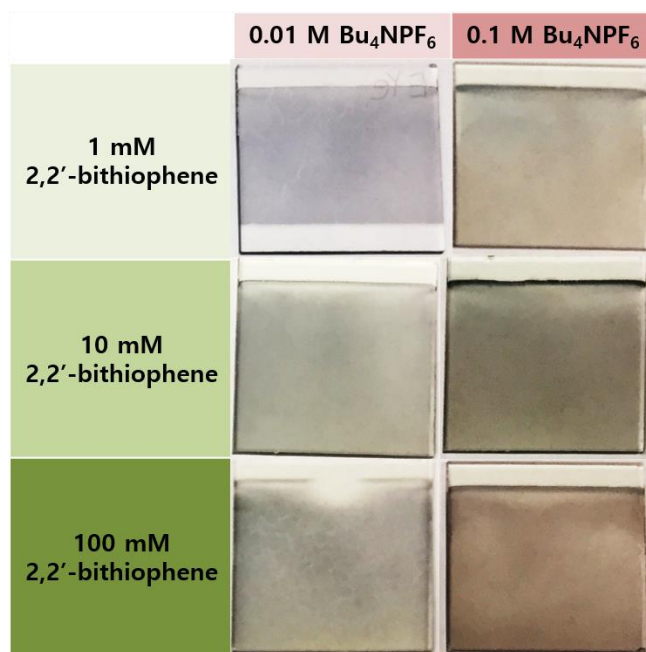


Figure 14. Photos of films synthesized in electrolytes of varying 2,2'-bithiophene and Bu_4NPF_6 concentrations. Width of image: 2.5 cm

2.2.3 Electrochemical biasing sequence

For the utilization of electropolymerized polythiophene as an HTL, the synthesis should not be needlessly long. Although cyclic voltammetry is a convenient technique for monitoring the polymerization process, it is time-consuming since most of the time is spent below the polymerization potential. Furthermore, due to its dynamic nature, it is difficult to investigate how film morphology is affected by a certain overpotential, polymerization duration, growth speed, etc. Therefore, potentiostatic and galvanostatic techniques were explored for further film optimization.

SEM cross-section imaging was used to assess the nanoscale uniformity. Generally, the film growth involved the formation of a compact uniform layer followed by non-uniform outgrowths, as shown in Figure 15.

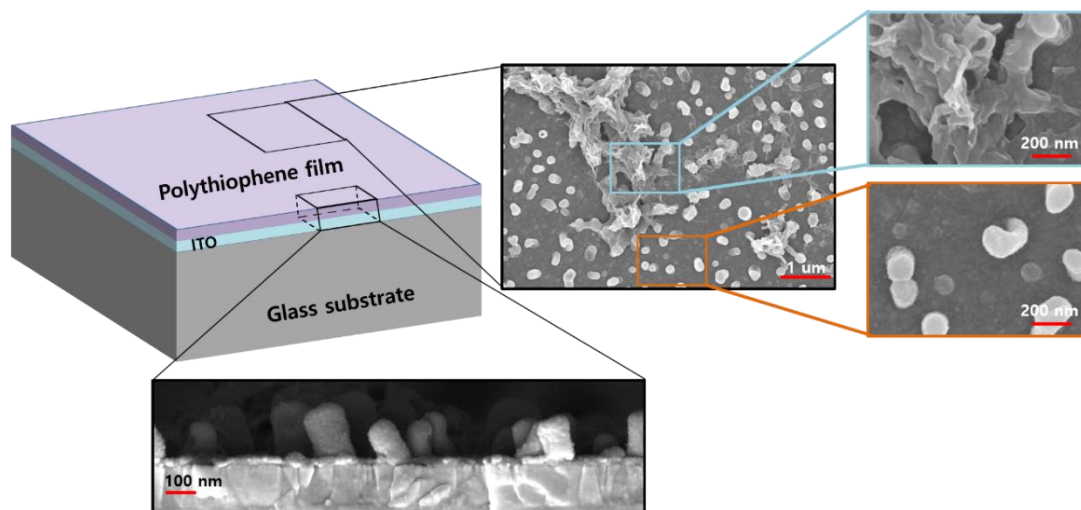


Figure 15. Polythiophene morphology before optimization

The outgrowths tended to become more exaggerated with longer polymerization duration, as shown in Figure 16. By limiting the quantity of delivered charge to 5 mC/cm², only the compact uniform layer was formed.

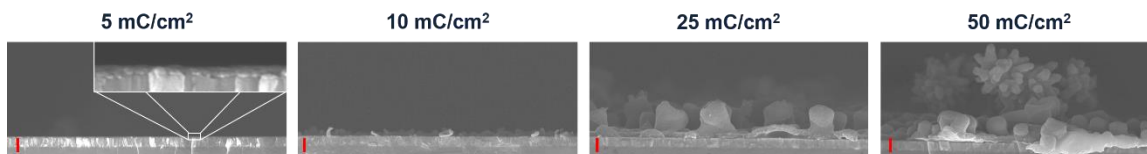


Figure 16. Cross-section SEM images of polythiophene films electropolymerized with different quantities of delivered charge during deposition. Scale bar: 200 nm

Potentiostatic polymerization allows one to investigate how overpotential affects film morphology. As seen in Figure 17, the film tends to develop non-uniform outgrowths at high overpotentials. Thus, uniformity can be retained for thicker films (>10 mC/cm²) by utilizing a slower growth rate.

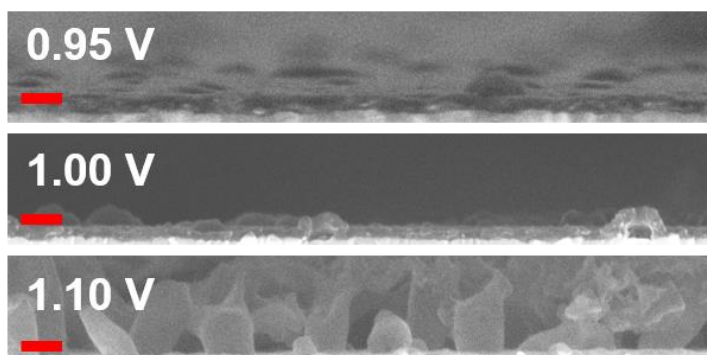


Figure 17. Cross-section SEM image of polythiophene films electropolymerized at different voltages vs Ag/Ag⁺ until reaching 10 mC/cm². Scale bar: 100 nm

Once an understanding of how biasing sequence affected film morphology had been developed, depositions were done through galvanostatic methods. Galvanostatic deposition is more attractive than potentiostatic deposition for industrial applications because it requires less sophisticated equipment^[22], does not require a reference electrode, and the thickness of the film can be precisely manipulated by controlling the duration of the deposition. Since uniform films were obtained at low overpotentials and low quantities of delivered charge, a low applied current density of 0.02 mA/cm^2 was used. The stabilized voltage during polymerization was $1.01 \text{ V vs. Ag/Ag}^+$. Cross-section SEM imaging verified that the parameters led to the formation of a uniform film (Figure 18).

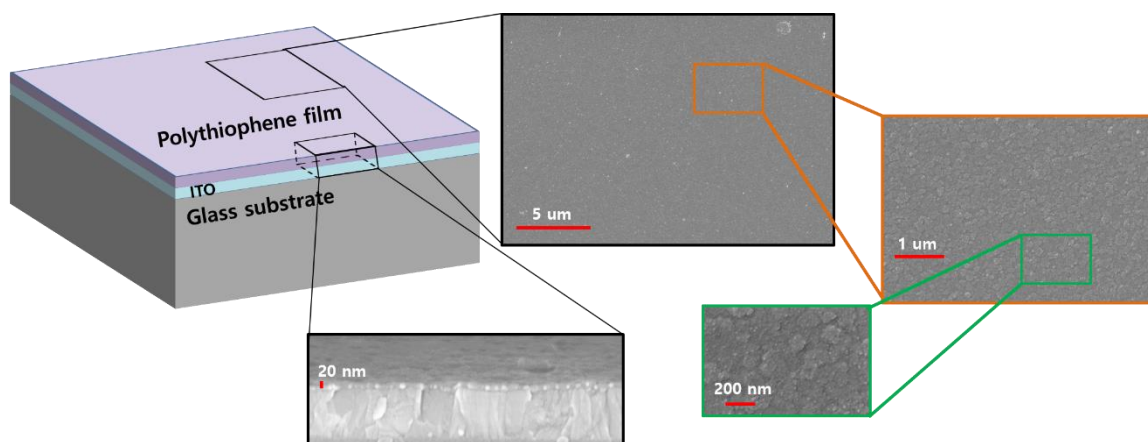


Figure 18. Polythiophene morphology for film synthesized with final parameters, i.e., constant current of 0.02 mA/cm^2 until reaching 3 mC/cm^2

2.3 Large-area deposition

The electrochemical parameters developed for $2.5 \times 2.5 \text{ cm}^2$ substrates were applied to a $10 \times 10 \text{ cm}^2$ substrate. The deposition was done at 0.02 mA/cm^2 until reaching 5 mC/cm^2 with a WE-CE separation of 0.5 cm (Figure 19a-c). The resulting film appeared uniform by naked eye (Figure 19d), although there was some red hue (i.e., undoped polythiophene) in the regions closest to the alligator clip. This non-uniform doping artifact can be easily mitigated by performing an additional doping step in thiophene-free electrolyte after polymerization.

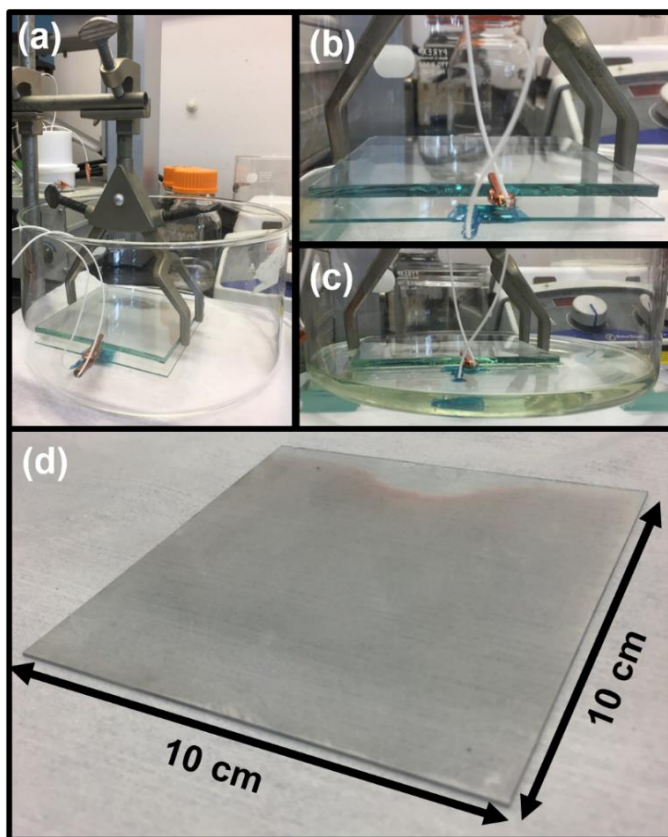


Figure 19. Polythiophene film deposition. (a,b,c) Electrochemical cell setup, before (a,b) and after (c) adding electrolyte. (d) $10 \text{ cm} \times 10 \text{ cm}$ polythiophene film deposited on ITO

The film was imaged at nine different regions of the film (Figure 20a) by SEM in top-view and cross-sectional view. Both confirmed that the film was highly uniform throughout the 10x10cm² area, although with some imperfections. Cross-section imaging (Figure 20b) revealed that the film thickness was similar in all areas, except for the top two corners where it was thinner. This may be avoided by positioning the electrical contacts in the corners rather than on the middle edge, so that the applied electrical potential is more evenly distributed. Top-view imaging (Figure 20c) revealed that there was complete film coverage in all regions, but with slightly rougher surface morphology close to the edges.

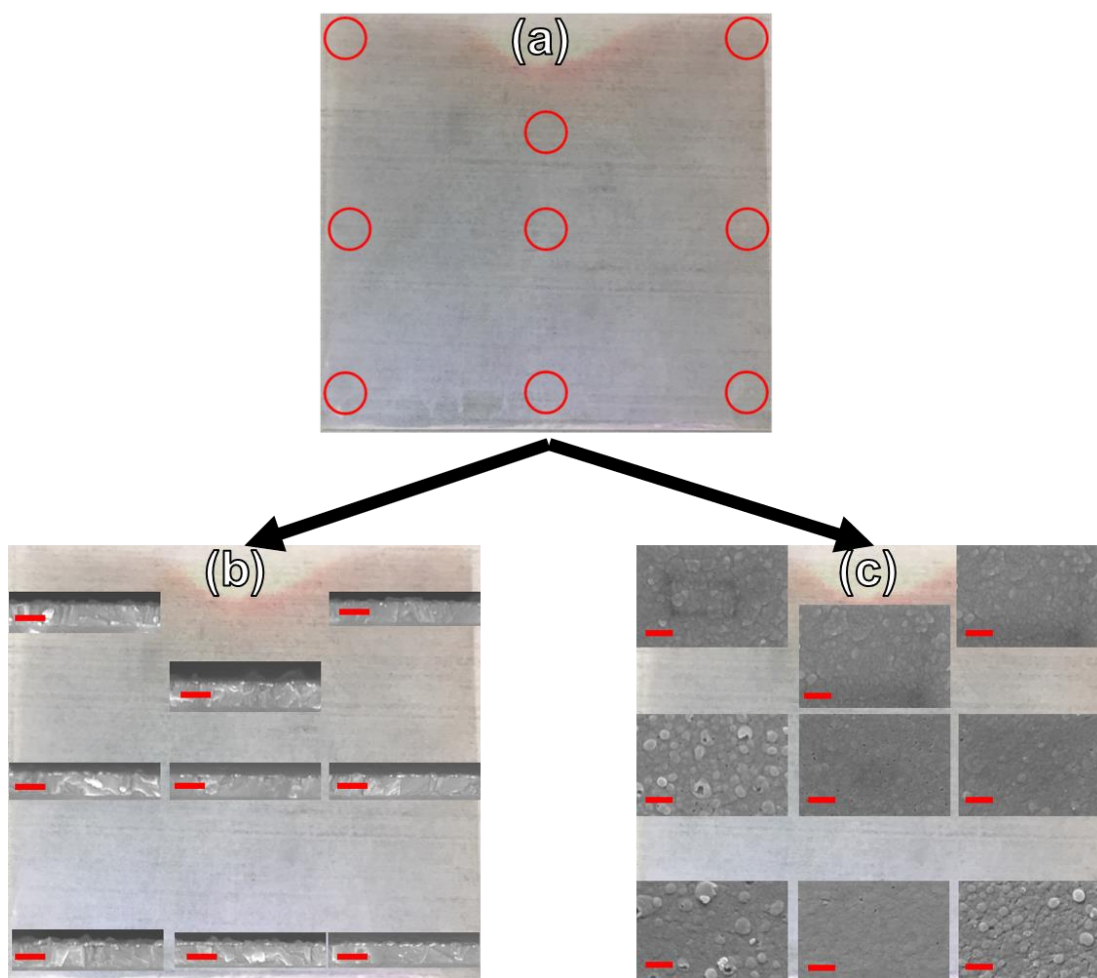


Figure 20. SEM imaging of 10x10cm² polythiophene film. (a) Inspected regions. (b) Cross-section imaging. (c) Top-view imaging

2.4 Summary

Polythiophene films have successfully been synthesized by electrochemical polymerization and optimized to produce uniform films on the milliscale and nanoscale. A 100 cm² deposition was demonstrated and proved the technique's ability to deposit highly uniform films on large substrates.

Chapter 3. Solar Cells

Next, the uniform polythiophene thin films were implemented into solar cells. In the PSC research field, two basic cell architectures are used; normal and inverted, as shown in Figure 21. Polythiophene films grown on ITO can be directly incorporated into inverted structure solar cells simply by depositing perovskite, electron-transporting layer (ETL), and current collector on top of it. The normal architecture design, on the other hand, is more challenging to utilize because it requires that the polythiophene is deposited on top of perovskite, which may degrade the perovskite in the process.

I began by implementing the films into the inverted cell setup, using JV curves and SEM imaging to get a general idea of how to optimize performance. Next, I explored the viability of the normal cell setup, performing tests to determine whether perovskite is compatible with in situ electrodeposition.

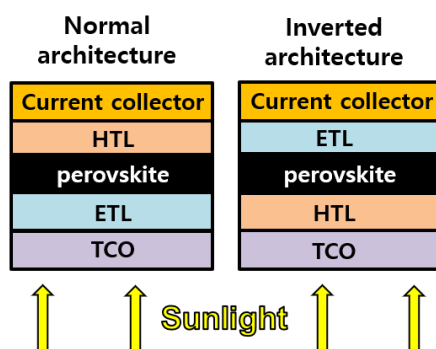


Figure 21. The two main types of PSC architectures. TCO: Transparent Conducting Oxide (i.e., ITO in this work)

3.1 Inverted Structure Solar Cells

Electrodeposited polythiophene has been implemented into inverted solar cells once before^[7], but, as mentioned in chapter 1, the reported method has weaknesses that must be addressed in order to make it suitable for industrial applications. First, boron trifluoride diethyl etherate (BFEE) was used as the electrolyte solvent, which is extremely hazardous, as it reacts with the moisture in air to generate lethally toxic and volatile hydrogen fluoride gas. As a secondary effect of this, the film deposition has to be performed in an argon atmosphere, which introduces costs associated with sustaining an inert atmosphere for chemical storage and film fabrication (i.e., purchase of glovebox, compressed gas cylinders, etc.). Second, the deposition was applied to $<1\text{cm}^2$ substrates and was thus never proven as a large-area deposition technique.

To attack these weaknesses, the considerably less toxic dichloromethane was used as the electrolyte solvent. Considering that dichloromethane is immiscible with water, the experiments could be performed in ambient air. Furthermore, the films were deposited onto 4.125 cm^2 regions, showcasing the utility of the technique for larger areas.

Since polythiophene is implemented as the HTL in the inverted architecture, light must pass through the polythiophene film before reaching the perovskite layer; thus, transmittance losses due to light absorption by polythiophene must be taken into account. Ultraviolet-visible (UV-Vis) spectroscopy (Figure 22) showed

that the transmittance of ITO on its own is 76-89% in the 375-850 nm wavelength range and dropped to 70-80% and 64-76% after polythiophene was deposited with 3.0 and 5.0 mC/cm² of delivered charge, respectively. Ideally, the HTL film should be as thin as possible to minimize these transmittance losses, but the electron-blocking ability of the film may be lost if the thickness approaches length scales where quantum tunneling can occur.

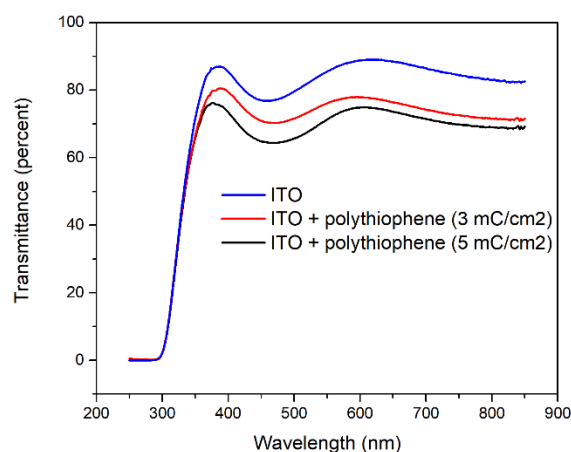


Figure 22. UV-Vis transmittance of polythiophene films of various thicknesses

3.1.1 Photoluminescence

Steady-state photoluminescence (ss-PL) measurements were taken in order to gain a preliminary idea of how polythiophene polymerized from 2,2'-bithiophene might perform as an HTL in PSCs.

A strong photoluminescence intensity indicates a greater rate of radiative recombination of electron-hole pairs, which in turn implies that non-radiative

pathways are repressed. Photoluminescence generally correlates with diffusion length of charge carriers within the film, and it is thus commonly used as a tool to evaluate material quality for a solar absorber material^[23]. In PSCs, the most significant non-radiative recombination pathway is Shockley-Read-Hall (SRH) (i.e., defect-assisted) recombination^[24]. This type of recombination occurs as a result of defect energy states within the bandgap, which facilitate the relaxation of excited charge carriers and spend the released energy as heat. Defects may be introduced by impurities in the material, local non-stoichiometry, or dangling bonds (i.e., under-coordinated atoms) at surfaces. In the last few years, surface passivation of dangling bonds at perovskite grain boundaries has proven to be an effective strategy towards achieving >20% PCEs^[5, 25,26].

Photoluminescence is also commonly used to assess the quenching ability of a charge-transporting material^[27]. For this purpose, perovskite is deposited on top of a charge-transporting layer and the PL intensity compared to that of perovskite on a low-quenching reference substrate (commonly ITO or glass). An intensity reduction may indicate that charges are efficiently transferred across the perovskite/charge-transporting layer interface, which enhances charge collection efficiency during solar cell operation. However, a common source of error is the possibility that the reduction may also result from an increase in surface recombination due to poor interfacial contact. Ss-PL should therefore not be used as the only method of characterization to evaluate a charge-transporting layer.

Perovskite was deposited on an ITO substrate that had half of its area covered by electrodeposited polythiophene. The PL peak (Figure 23) was at 770 nm in both cases, confirming that the perovskite had successfully formed in both regions. The PL peak intensity was reduced by a factor of 47 on top of polythiophene relative to the low-quenching region. This served as a preliminary verification that the film facilitated hole transfer across the HTL/perovskite interface, but as discussed before, it does not conclusively determine whether the reduction was mainly due to quenching or introduction of defects to the interface.

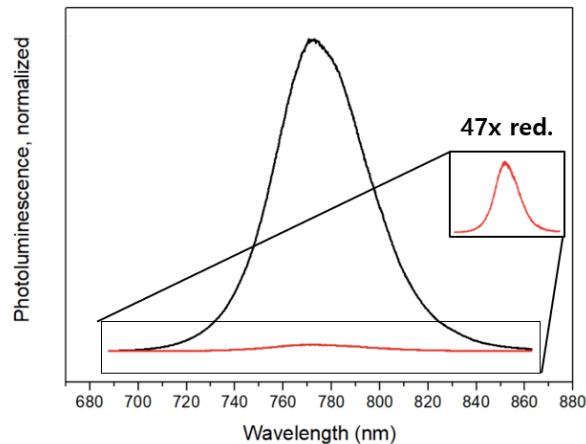


Figure 23. Ss-PL measurements of MAPbI₃/polythiophene/ITO

3.1.2 Implementation into Solar Cells

Polythiophene films were implemented into inverted structure solar cells as a targeted approach to verify whether they performed as an HTL in PSCs. The device architecture employed was ITO/polythiophene/MAPbI₃/phenyl-C₆₁-butyric acid methyl ester (PCBM)/Au. The simple glass cell setup was used with a 10

mM 2,2'-bithiophene / 0.1 M Bu₄NPF₆ / DCM electrolyte. The solar cell performance was diagnosed by running current density – voltage (JV) scans under AM1.5G illumination (100 mW/cm²), where current density was recorded while voltage was swept from short-circuit (0 V) to open-circuit (V_{oc}).

The JV curves exhibited the characteristic shape expected for a photovoltaic device (Figure 24a), and thus confirmed that polythiophene successfully performed its role as an HTL, i.e., it demonstrated hole-accepting, hole-transporting, and electron-blocking properties. PCEs were normally in the 4.0 - 4.5% range (Figure 24b), with the champion cell demonstrating a 6.97% PCE (Figure 24a).

The champion cell had a high short-circuit current density (J_{sc}) of 19.0 mA/cm², a mediocre open-circuit voltage (V_{oc}) of 0.77 V, and a poor fill factor (FF) of 47.5%. The low FF and V_{oc} imply a low shunt resistance (R_{shunt}), i.e., a low resistance for the undesirable current pathways within the cell. These may be represented by recombination events where the excited electron goes into a 'dead-end' energy state that does not lead out to the current collectors, e.g., going from the perovskite conduction band minimum (CBM) to the HTL valence band maximum (VBM) (see Figure 25). The electron may also go to defect states within the bandgap that have formed as a result of poor interfacial contact.

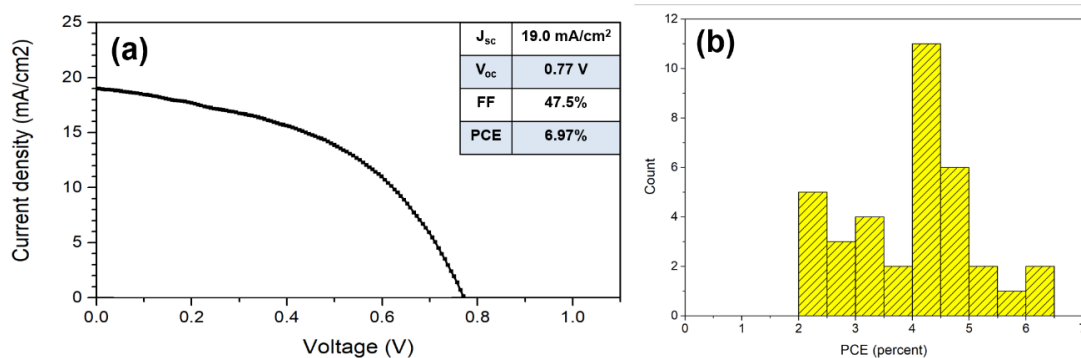


Figure 24. Solar cell performance of inverted structure PSCs with polythiophene as the HTL. (a) JV curve and PV parameters of the champion cell. (b) Histogram of PCE efficiencies

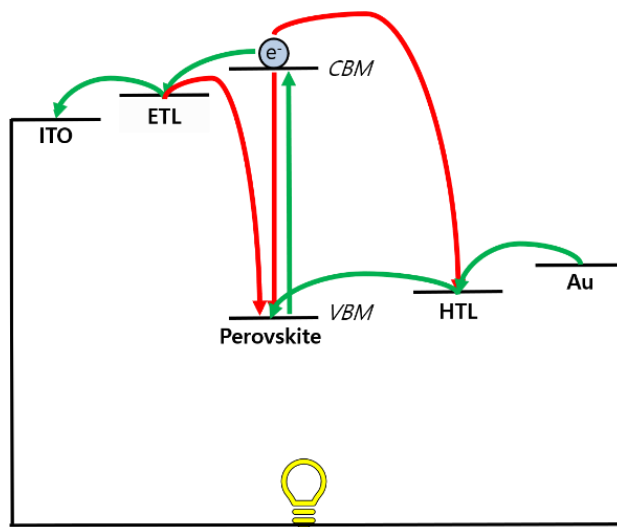


Figure 25. Possible current pathways for an excited charge in a PSC. Undesirable pathways (shunt current, i.e., recombination) are marked in red and the desired pathway (photovoltaic current) is marked in green. Pathways due to incomplete coverage of layers (e.g., from ETL to HTL due to the two layers coming in direct contact as a result of pinholes in perovskite film) or defects (e.g., as a result of poor interfacial contact) are not included

3.1.3 Imaging of Polythiophene/Perovskite Interface by SEM

SEM cross-section imaging was performed to better understand whether poor interfacial contact between polythiophene and perovskite was responsible for

the lack of performance. The imaging revealed that, although there was mostly good contact between the perovskite and HTL, there were also voids present (Figure 26). Loss of hole-transfer ability at these sites, as well as the additional surface area introduced, may increase the rate of SRH recombination, which would explain the high shunt resistance observed in the champion cell JV curve. Thus, the PSC performance may be improved if a more conformal contact is established at the polythiophene/perovskite interface, which can be achieved by 1) minimizing nanoscale film roughness, so that non-uniformities do not interfere with perovskite grain crystallization (explored in section 2.2.3), and/or 2) enhance wetting of perovskite precursor solution on polythiophene (e.g. through the use of a hydrophilic interlayer). For the latter strategy, an appropriate surface treatment may help establish conformal interfacial contact between the perovskite and HTL by tuning the polythiophene surface energy so that the perovskite precursor solution has just the right degree of wetting with the polythiophene substrate during deposition^[28].

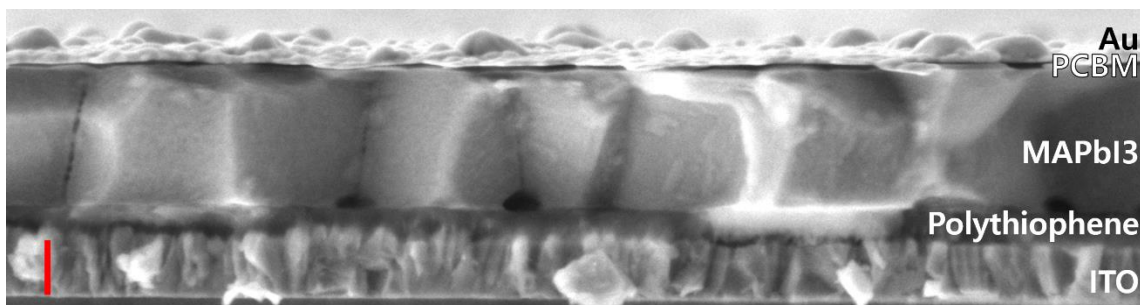


Figure 26. Cross-section SEM image of inverted structure PSC with electrodeposited polythiophene. Scale bar: 100 nm

3.1.4 Economic Analysis

An economic analysis was performed to evaluate the promise of the developed method as a scalable tool for HTL deposition in PSC fabrication. Commercial photovoltaic cells are usually priced according to their energy-generating capabilities, i.e., in US dollars per watt (\$/W). Silicon photovoltaic cells made in the United States, for example, have a manufacturing cost of \$0.28/W^[29]. This metric is flawed for comparing the method developed in this project to existing technologies since the energy-generating capability of the electrodeposited HTL is yet to be optimized. Thus, in this analysis, the energy-generation aspect was ignored, and the manufacturing cost of the HTL evaluated by determining the area-dependent cost (\$/m²). The previously mentioned cost of \$0.28/W for silicon solar cells converts to an area-dependent cost in the range of \$42-56/m² for 15-20% PCEs. Using currently established methods, the estimated manufacturing cost of PSCs is \$90/m² (assuming silver is used instead of gold as the current collector)^[30]. The HTL makes up the largest portion of this cost (even more than silver) with a cost of \$18/m² for the material alone (not including deposition equipment, labor, etc.), assuming a 95% material utilization rate.

To calculate the manufacturing cost, costs of materials, capital investments, and operation (electricity and labor) were determined and added together according to the equation shown below:

$$\begin{aligned}
& \text{Manufacturing Cost } (\$/m^2) \\
& = \\
& \quad \text{Materials Cost } (\$/m^2) \\
& \quad + \\
& \quad \text{Total Capital Cost } (\$) \\
& \frac{\text{Annual Production Rate } (m^2/y) \times \text{Plant Lifetime } (y)}{\quad} \\
& \quad + \\
& \quad \frac{\text{Annual Operating Costs } (\$/y)}{\text{Annual Production Rate } (m^2/y)}
\end{aligned}$$

3.1.4.1 Material Costs

First, the material cost for electrodeposited polythiophene in the inverted structure solar cells from the previous section was calculated. For this deposition, a 1 mM 2,2'-bithiophene / 0.01 M Bu₄NPF₆ / DCM electrolyte was used. The cost of each electrolyte component is ¢0.0406/mL, ¢0.4505/g, and ¢0.2178/g for DCM (Alibaba.com), Bu₄NPF₆ (TCI Chemicals), and 2,2'-bithiophene (Sigma-Aldrich), respectively, totaling ¢0.7478/mL for the electrolyte (see Figure 27a). With a WE-CE spacing of 0.5 cm, the volume of electrolyte needed to fill the gap is 0.5 mL per cm²; thus, the electrolyte cost can be converted into an area-dependent cost of \$35.53/m² (the electrolyte was used only once before being discarded) (see Figure 27b).

For the champion cell, 2 mC/cm² of charge was delivered, which means that only ~4% of the 2,2'-bithiophene present in the electrolyte was utilized. Even a modest improvement in the material utilization rate can drastically reduce the cost, e.g., a 20% utilization rate will drop the cost to \$7.11/m², i.e., a fifth of its initial value. This can be achieved by having a lower quantity of 2,2'-bithiophene present,

either by employing a lower concentration or narrowing the WE-CE gap so that a smaller volume of electrolyte is within the gap.

Additionally, some fraction of the Bu_4NPF_6 concentration is consumed to supply dopant ions to stabilize positive charges on the polythiophene chain; in this project, ~5% of the charge delivered during polymerization could be attributed to film doping. Therefore, a 2 mC/cm^2 deposition would indicate that $\sim 0.1 \text{ mC/cm}^2$ of the delivered charge was due to PF_6^- migration into the film, which means that only 0.02% of the total amount of Bu_4NPF_6 is consumed. To further lower the cost, the Bu_4NPF_6 concentration may be lowered to a level where the quantity better matches the number of ions needed to perform the doping, or, alternatively, a method for recycling the Bu_4NPF_6 across sequential depositions may be implemented.

Lastly, the DCM solvent is not consumed at all in the deposition process. Recycling (e.g., through distillation) can here provide a way to make the DCM component of the electrolyte cost negligible relative to the cost of the 2,2'-bithiophene and Bu_4NPF_6 .

If the material utilization of the 2,2'-bithiophene and Bu_4NPF_6 is increased to ~100% and efficient recycling methods are implemented for the DCM solvent so that the cost is negligible compared to that of the remaining electrolyte components, then the total material cost converges to a theoretical minimum cost of $\$0.4336/\text{m}^2$, as shown in Figure 27c. This cost is for a 2 mC/cm^2 -deposited film,

so it is proportional to film thickness; e.g., a 10 mC/cm²-deposited film will have a minimum material cost of \$2.168/m².

This cost compares well with previous methods, where the HTL material has been estimated to cost \$18/m² [30]. It should be mentioned, however, that this cost is still likely to be inflated since it assumes that the Bu₄NPF₆ and 2,2'-bithiophene are bought from research-scale suppliers. Given that an industrial-scale supplier of these chemicals is available, such that the price drops due to the increased volume of production, the actual cost would be even lower.

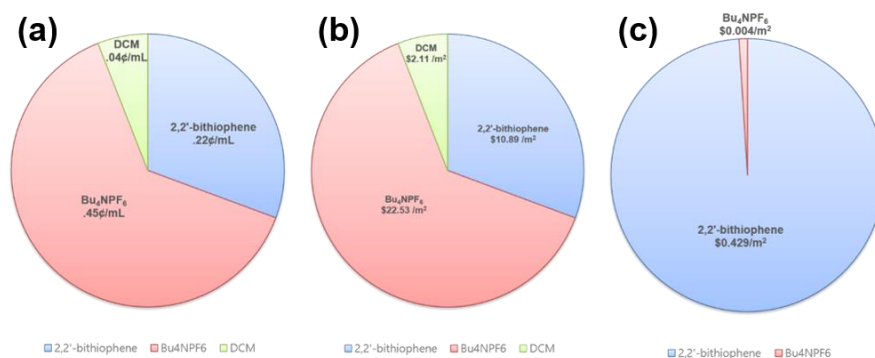


Figure 27. Material cost for each component of electrolyte required to electrodeposit polythiophene. (a) Cost per mL for 1 mM 2,2'-bithiophene / 0.01 M Bu₄NPF₆ / DCM electrolyte. (b) Cost per square meter for depositing polythiophene from 1 mM 2,2'-bithiophene / 0.01 M Bu₄NPF₆ / DCM electrolyte, assuming the electrolyte is discarded after a single deposition. (c) Cost per square meter for depositing polythiophene, assuming 100% material utilization and cost-effective recycling of DCM

3.1.4.2 Capital and Operational Costs

In addition to the raw material costs, the electrodeposition method requires the use of a device to supply current. A single-channel potentiostat can be acquired

for \$3000^[31], and the impact of this capital cost on the economics of the electrodeposition process can be evaluated by taking into account the useful lifetime of the instrument and the annual production rate.

First, the useful lifetime was defined as the years of warranty protection provided by the manufacturer, which was 2 years. Second, the annual production rate was calculated based on experimental parameters set in the previous sections and constraints related to factory operation. The throughput is limited by the rate of deposition and the quantity of deposited material. Assuming a current of 0.02 mA/cm² and 2 mC/cm² of delivered charge, it will take 1 min 40 sec (100 sec) to perform deposition on a single substrate. For simplicity, it was further assumed that the downtime in between depositions (i.e., the time spent to switch electrical connections to next substrate, replenish electrolyte, etc.) was 1 min 40 sec as well, resulting in 3 min 20 sec (200 sec) per deposition. If 100 cm² substrates are used for the depositions, then the throughput is 0.18 m²/hr. For a factory that is in operation 8 hours a day, 5 days a week, and 44 weeks a year, the throughput converts to a production rate of 317 m²/yr.

Finally, the area-dependent capital cost was calculated by taking the capital cost of the single potentiostat (\$3000) and dividing by the product of its useful lifetime (2 years) and annual production rate (317 m²/yr), which yielded a cost of \$4.73/m². It is possible that this cost can be significantly reduced by investing in simpler current-control devices; since the deposition process only requires the supply of constant current, the added functionality of research-scale potentiostats

may be redundant, so that it would be more economical to build simple constant current devices from cheap components.

The throughput of $0.18 \text{ m}^2/\text{hr}$ is quite slow compared to other candidates for scalable film deposition in PSCs, which are generally in the range $17\text{-}84 \text{ m}^2/\text{hr}$ ^[30]. For an industrial-scale operation, the throughput needs to match or exceed this rate^[32]. This can be achieved by purchasing multiple-channel potentiostats; 50 times as many channels will yield a 50 times as high production rate. The previously calculated area-dependent capital cost is independent of the number of channels, so the production rate can be increased without compromising the capital cost.

Lastly, the costs associated with daily operation were considered, i.e., electricity and labor. For my system, pushing a constant current of $0.02 \text{ mA}/\text{cm}^2$ through a 100 cm^2 ITO substrate placed 0.5 cm away from the CE led to a stabilized voltage of 2.4 V . As a result, 4.8 mW of electricity was consumed for a 100 cm^2 deposition, which converts to an energy consumption of $13.33 \text{ mWh}/\text{m}^2$ (energy usage = $4.8 \text{ mWh}/\text{hr}$; production rate = $0.36 \text{ m}^2/\text{hr}$). By taking the average spot price for industrial electricity in California on 4 Dec 2019 ($\$104.9$)^[33], the cost of electricity was found to be $\$0.0000014/\text{m}^2$, which is negligible compared to the material and capital costs. This is a testament to the energy efficiency of electrochemical synthesis; the electrical energy can be extremely efficiently directed towards driving the desired chemical reaction and thus offers a pathway to maximize the energy efficiency of material manufacturing processes.

Labor costs also add to the operational costs. Between successive electrodepositions, the ITO substrate and electrolyte must be replaced. If 1 laborer is employed per channel to perform this task with a salary of \$15/hr, then the cost of labor that goes into each square meter of deposited film is \$83.33. This cost item alone is nearly double that of the total manufacturing cost of silicon solar cells (\$42-56/m² [29]) and thus threatens to make the electrodeposition method economically unviable. Thus, it will be necessary to develop automated systems so that laborers are not needed to switch out substrates and electrolyte between depositions, e.g., by installing robot arms, which would further increase capital costs. In this way, the workers can focus on other tasks such as maintenance of the equipment and ensuring that the automated systems work properly. By having 1 worker for each set of 25 channels, the cost drops to \$3.33/m²; this assumes that all tasks related to normal operation of the manufacturing process and maintenance of equipment are included in the duties of these workers.

3.1.4.3 Total Manufacturing Cost

By adding up the material, capital, and operational costs, a final HTL manufacturing cost of \$8.49/m² was calculated (see Figure 28). This cost does not take into account material wastage or additional capital costs due to automation, but the analysis nevertheless serves as a useful case study for evaluating the economic viability of the electrodeposition method and provides clues in regards to the primary roadblocks inhibiting its application towards industrial-scale

production. The method appears to enable cheaper HTL fabrication than previous methods ($\$8.49/\text{m}^2$ total manufacturing cost vs. $\$18/\text{m}^2$ for material only^[30]) and shows potential for becoming even cheaper, e.g., by using lower-cost current-control devices. This may assist in bringing the manufacturing cost of the complete PSC down towards (and perhaps below) the level of commercial photovoltaic cells, such as those based on silicon ($\$42\text{-}56/\text{m}^2$ ^[29]).

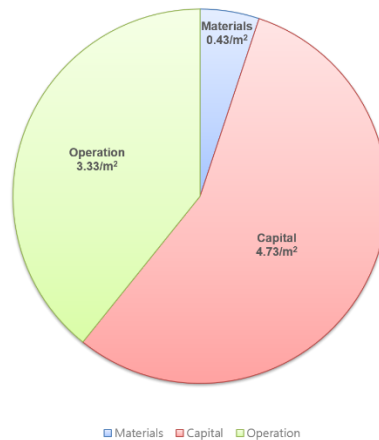


Figure 28. Manufacturing cost of electrodeposited polythiophene as HTL

3.1.5 Future promise and Critical Analysis

Inverted structure PSCs with electrodeposited polythiophene has the potential to become a scalable method for HTL fabrication as it utilizes cheap precursors, is compatible with large-area substrates, uses less toxic chemicals than previously published results, and is not dependent upon an inert atmosphere for synthesis.

Nevertheless, the performance of the electrodeposited HTL must be improved before the technique is proven as a viable method; <7% PCE is not high enough for industrial application and should get to at least >15% before it is ready for implementation^[34]. It is possible that some drastic changes may have to be made to the material system to achieve this, e.g., solvent, supporting electrolyte, choice of building block, etc. Perhaps the 2,2'-bithiophene building block is not conducive to forming a film of the appropriate properties; in that case, other precursors might have to be explored, e.g., 3,4-ethylenedioxythiophene (EDOT) to form PEDOT, or perhaps even move away from polythiophene entirely, using aniline to synthesize polyaniline, for example.

Even if the performance is improved to an acceptable level, the issue remains that an inverted architecture PSC requires the use of an ETL deposition method that is non-corrosive to perovskite. This imposes stringent requirements to the materials that can be used as an ETL, and most of the available options (including PCBM used in this work) are just as expensive as the HTL materials that the polythiophene was aiming to replace. This issue can be overcome by either 1) finding a cheaper ETL candidate that is compatible with the perovskite substrate (research is undergoing on finding new ETL alternatives^[35,36]), or 2) finding a way to deposit the polythiophene on top of perovskite, allowing for the use of cheap ETLs in normal structure PSCs.

3.2 Normal Structure Solar Cells

The promise in electrodepositing polythiophene onto perovskite lies in that it enables the use of well-established, cheap, high-performance ETLs. Titanium dioxide (TiO_2) and tin oxide (SnO_x) have already been incorporated as ETLs in high-performance PSCs^[5,26] and utilize cheap precursors, but unfortunately, the high temperatures required for crystallization make them incompatible with deposition onto perovskite, leaving only expensive materials left as options for ETLs in inverted structure PSCs. If a cheap HTL could be deposited onto perovskite without damaging it in the process, it would allow for the use of a cheap ETL such as TiO_2 or SnO_x , so that the overall cost of the ETL/perovskite/HTL part of the solar cell would likely be in the required range for commercialization.

This strategy has been explored once before; Samu et al. electropolymerized PEDOT from its dimer (bis-EDOT) onto MAPbI_3 perovskite for use as the HTL in normal structure PSCs^[37]. The methodology did not entirely prevent damage to the perovskite, as it exhibited slight degradation as a result of the electrodeposition process. The champion cell performance (5.9% PCE) was attained by minimizing the duration of the applied bias to limit the extent of degradation. If electrodeposited polythiophene is to be viable for use in normal structure PSCs, then experimental parameters should be established that entirely prevent perovskite degradation.

For the in-situ electropolymerization of polythiophene onto perovskite, there are two primary degradation pathways that must be avoided: chemical interaction with the electrolyte and electrochemical over-oxidation. Both depend on the type of perovskite used and the composition of the electrolyte that it is in contact with.

I investigated how electrolyte composition can be manipulated to lower the polymerization potential below the degradation potential of perovskite and performed chemical and electrochemical stability tests of perovskite in the electrolytes with the lowest polymerization potential. The goal was to establish conditions that would allow for the electrochemical growth of polythiophene directly onto perovskite from a solution of thiophene oligomers.

3.2.1 Designing Electrolytes with Low Polymerization Potentials

The applied voltage to initiate polymerization should not lead to degradation of the perovskite, i.e., the polymerization potential of the electrolyte should be below the degradation potential of the perovskite. As discussed in section 2.2.2.1, the polymerization potential can be lowered by using a longer-chain oligomer as the building block for polymerization, increasing oligomer concentration, or adding a Lewis acid to the electrolyte. These strategies were implemented into the electrolyte design, and the electrolytes with the lowest polymerization potential were then chosen for subsequent chemical and electrochemical stability tests.

Cyclic voltammetry (CV) scans were employed in a range of electrolyte compositions to gain a general understanding of how polymerization potential

could most effectively be downshifted. The variables investigated were oligomer selection, oligomer concentration, and Lewis acid additive. DCM and Bu_4NPF_6 (0.1 M) were used as solvent and supporting electrolyte, respectively, as they are already well-established in literature as minimally corrosive to halide perovskites^[38]. ITO was used as the working electrode.

The first anodic sweep of the CV scan was used to determine the polymerization potential. As the voltage is swept in the positive direction, there is a weak upward slope corresponding to capacitive current below the polymerization potential, followed by a sharp current rise after the polymerization potential corresponding to faradaic current (Figure 29a), i.e., radicalization of thiophene, which leads to polymerization. The polymerization potential was defined as the intercept between the tangent lines of the two current slopes (Figure 29b).

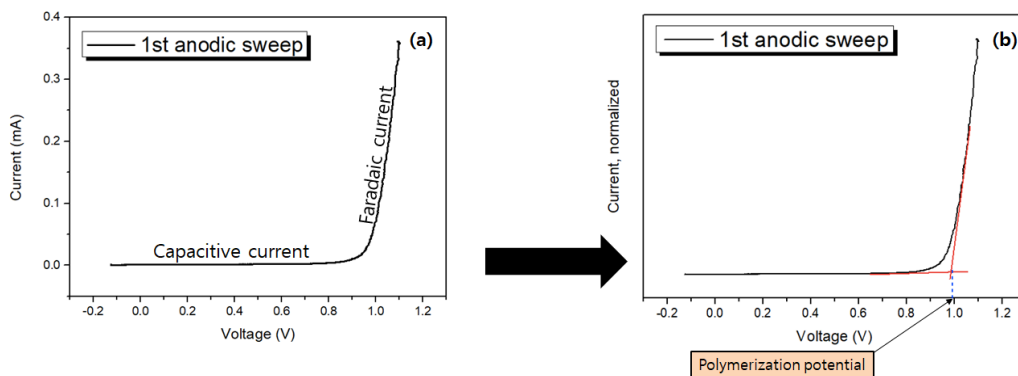


Figure 29. (a) A typical example of the first anodic sweep of a cyclic voltammetry electropolymerization. (b) Methodology for how polymerization potential for a given electrolyte composition is found

The results indicated that the most effective way to lower the polymerization potential was to use longer-chain thiophene oligomers (see Figure 30a). Replacing the thiophene dimer with the thiophene trimer of the same concentration led to a substantial downshift in polymerization potential of 250 mV (from 1.00 to 0.75 V vs. Ag/Ag⁺) (Figure 30b). The second most effective way was to increase the concentration of the oligomer; increasing the concentration from 10 mM to 100 mM of thiophene dimer led to a polymerization potential downshift of 70 mV. Lastly, even large concentrations (1 M, i.e. 12 v/v%) of the Lewis acid BFEE only had a modest impact, downshifting the polymerization potential by 50 mV.

The 100 mM dimer electrolyte and 10 mM trimer electrolyte were chosen for chemical and electrochemical compatibility tests with perovskite due to their low polymerization potentials. They are hereby referred to as the dimer and trimer electrolyte, respectively.

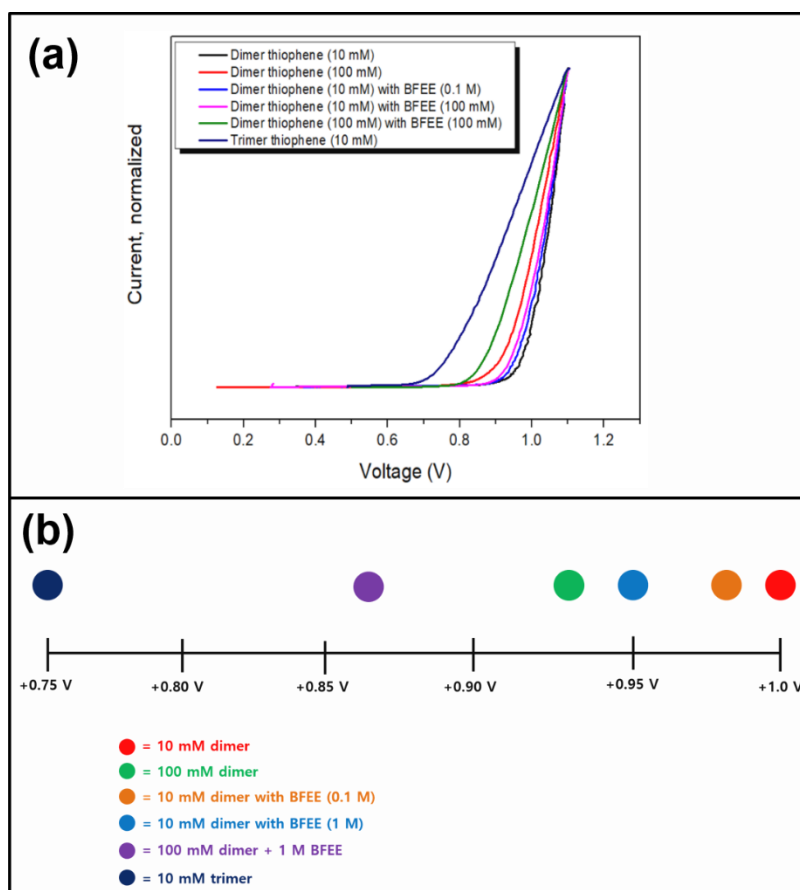


Figure 30. (a) First anodic sweep of CV scan in various electrolyte compositions. (b) Overview of polymerization potentials for various electrolyte compositions. Voltages referenced against Ag/Ag^+

3.2.2 Chemical Stability Tests

Methylammonium lead iodide (MAPbI_3) and mixed-cation ($\text{Cs}_{0.05}\text{FA}_{0.79}\text{MA}_{0.16}$) $\text{Pb}(\text{Br}_{0.16}\text{I}_{0.84})_3$ perovskite films were immersed for 30 min in the dimer (100 mM 2,2'-bithiophene) and trimer (10 mM 2,2':5',2''-terthiophene) electrolytes discussed in the previous section. After immersion, XRD of the tested

perovskites was taken to determine whether degradation had occurred. Both types of perovskite can be identified by a diffraction peak at 14.1°.

Mixed-cation perovskites ($(\text{Cs}_{0.05}\text{FA}_{0.79}\text{MA}_{0.16})\text{Pb}(\text{Br}_{0.16}\text{I}_{0.84})_3$) were found to be chemically unstable in both dimer and trimer electrolytes, as the XRD plots (Figure 31a) exhibited a peak at 11.6°, corresponding to the photo-inactive δ -phase of FAPbI_3 ^[39]. The peak for lead iodide at 12.7°, a common degradation product of perovskites^[38], was of weak intensity, indicating that the material was not corroded, but that it instead suffers from phase instability in contact with the electrolytes. It is, therefore, incompatible with electropolymerization in these electrolytes.

Methylammonium lead iodide (MAPbI_3) perovskite was found to be chemically stable in both dimer and trimer electrolytes. The peak for PbI_2 at 12.7° did not appear after immersion in either electrolyte (Figure 31b), indicating that MAPbI_3 is chemically compatible with these electrolytes. Since MAPbI_3 is not a mixed perovskite, phase instability was not an issue. Thus, MAPbI_3 was explored for further electrochemical compatibility tests.

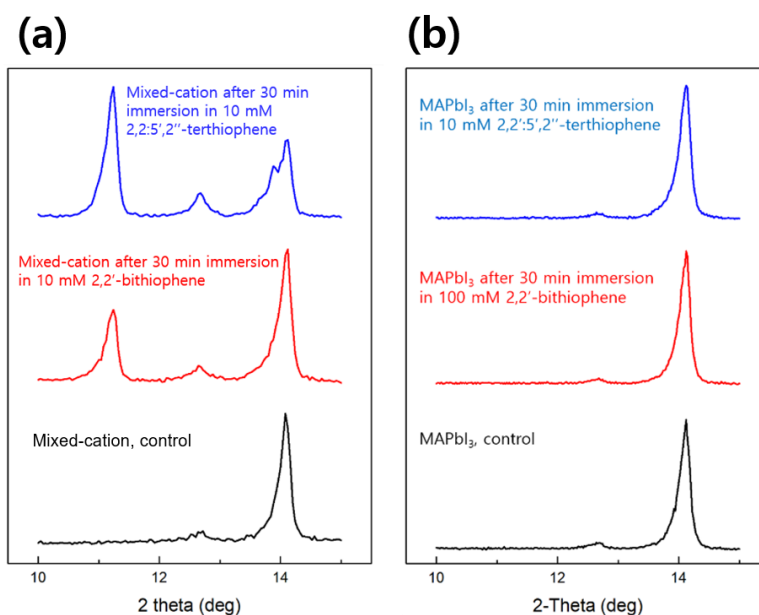


Figure 31. XRD plots of perovskite films after chemical stability tests for (a) $(\text{Cs}_{0.05}\text{FA}_{0.79}\text{MA}_{0.16})\text{Pb}(\text{Br}_{0.16}\text{I}_{0.84})_3$ and (b) MAPbI_3

3.2.3 Electrochemical Stability Tests

MAPbI_3 was electrochemically tested in dimer and trimer electrolytes, using MAPbI_3 on ITO as the working electrode. Samu et al. developed general parameters for conducting electrochemical experiments on MAPbI_3 , concluding that voltages up to 0.55 V can be applied for experiment durations up to 1 hour without causing significant damage to the perovskite^[38]. Considering that the electrodeposition happens within <5 min, the electrochemical tests were performed at similarly short time-scales in order to clarify how high potentials can be applied without causing degradation.

3.2.3.1 Identifying Corrosion Events by Cyclic Voltammetry

CV scans were used to identify the potentials at which corrosion occurred in each electrolyte. Scans up to 0.95 V vs. Ag/Ag⁺ were performed in the dimer electrolyte so that it was briefly above the polymerization potential (0.93 V) every cycle. The same upper range was chosen for the trimer electrolyte in order to make the results more easily comparable. In the first anodic sweep (Figure 32), a linear increase in current began at 0.4 V vs. Ag/Ag⁺ in both electrolytes, reaching 0.08 mA/cm² at 0.5 V, while faint redox peaks appeared at 0.58 and 0.75 V in the dimer and trimer electrolyte, respectively.

Upon subsequent cycles, the voltammogram for the trimer electrolyte displayed characteristics of polymerization, as a new redox peak appeared at 0.48 V, which grew with each cycle. The voltammogram for the dimer electrolyte exhibited no signs of polymerization. Considering that the trimer electrolyte has a much lower polymerization potential than the dimer electrolyte (0.75 V), additional CV scans were performed with an upper range of 0.80 V. In this case, the same characteristic voltammogram shape appeared, but with a more subdued current response; the de-doping peak at 0.28 V had a magnitude of 0.11 mA/cm² in the fifth cycle, which was 0.26 mA/cm² at the same stage when scanning up to 0.95 V. This indicates that more polymer was formed with the higher scan range, which

makes sense considering that more time was spent above the polymerization potential.

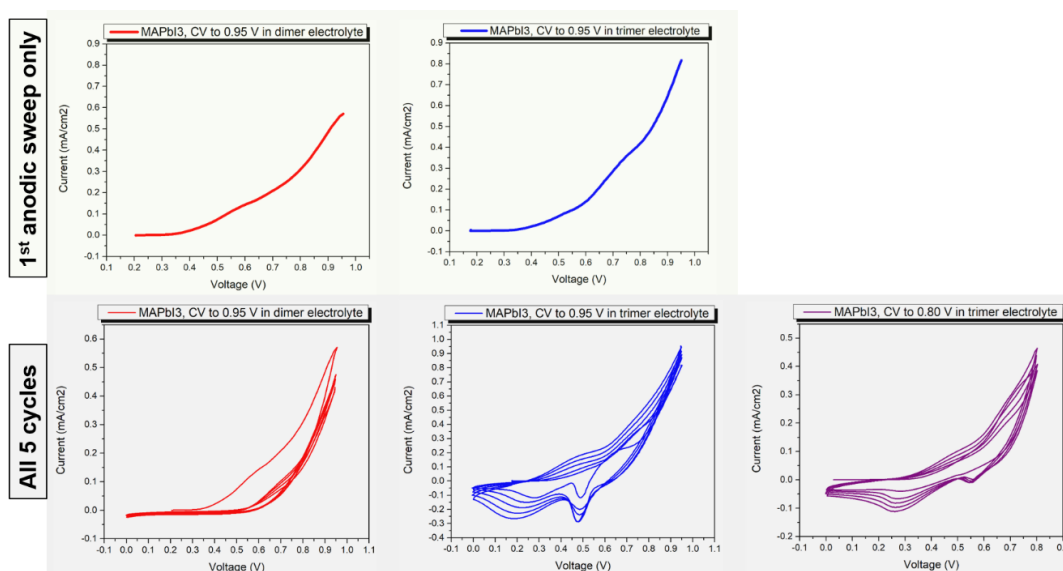


Figure 32. CV scans with MAPbI₃ on ITO as the working electrode in dimer and trimer electrolytes

XRD measurements revealed the presence of a diffraction peak at 12.7° for all three tested films (Figure 33), which matches with PbI₂. The perovskite diffraction peak was mostly retained for all three films, indicating that even prolonged biasing above the degradation potential does not allow the MAPbI₃-to-PbI₂ reaction to go to completion. It is possible that the PbI₂ is only being formed at the film surface in contact with the electrolyte, preventing the film bulk from being affected. Nevertheless, the fact that there is PbI₂ formation at all indicates that milder electrochemical conditions should be used to perform in situ electropolymerization onto perovskite.

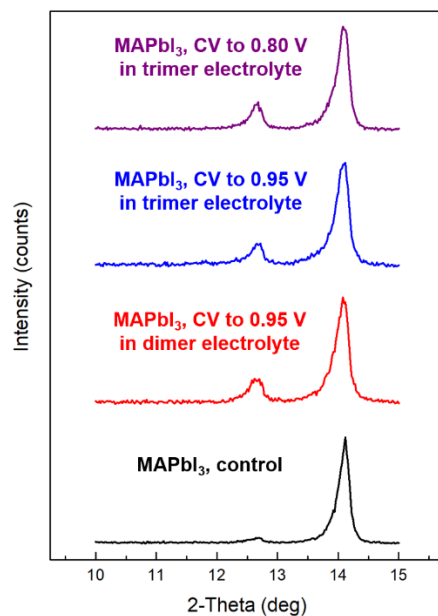


Figure 33. XRD of MAPbI₃ after CV scans in dimer and trimer electrolytes

3.2.3.2 Potentiostatic and Galvanostatic Studies

In order to establish a safe voltage window for MAPbI₃ perovskite, constant potential corrosion tests were performed. A range of voltages were applied to MAPbI₃ films for 2 min and was found to cause no visible difference to the film when the bias was 0.70 V vs. Ag/Ag⁺ or lower. The XRD plot of the film biased at 0.70 V matched that of the control perovskite, further strengthening the claim that MAPbI₃ is stable up to this voltage. Thus, it can be concluded that the redox peak at 0.58 V in the first anodic sweep of the CV scan does not represent a degradation event in the film.

When biased at 0.75 V, the film had a drastic change in appearance, exhibiting obvious degradation. Surprisingly, the change in appearance was not due to the formation of PbI_2 , which is easily noticeable due to its vibrant yellow color and usually expected to be the primary degradation product in corrosion studies. Instead, the film retained its black color, but with a more matte appearance (Figure 34b). The XRD plot showed no signal for the characteristic diffraction peak of PbI_2 at 12.7° , but instead revealed a peak at 9.16° (Figure 34a). This peak was not found to match any of the expected degradation products (PbI_2 , I_2 , Pb^0 , etc.). The low angle of diffraction implies that the degradation product must have long-range structural order.

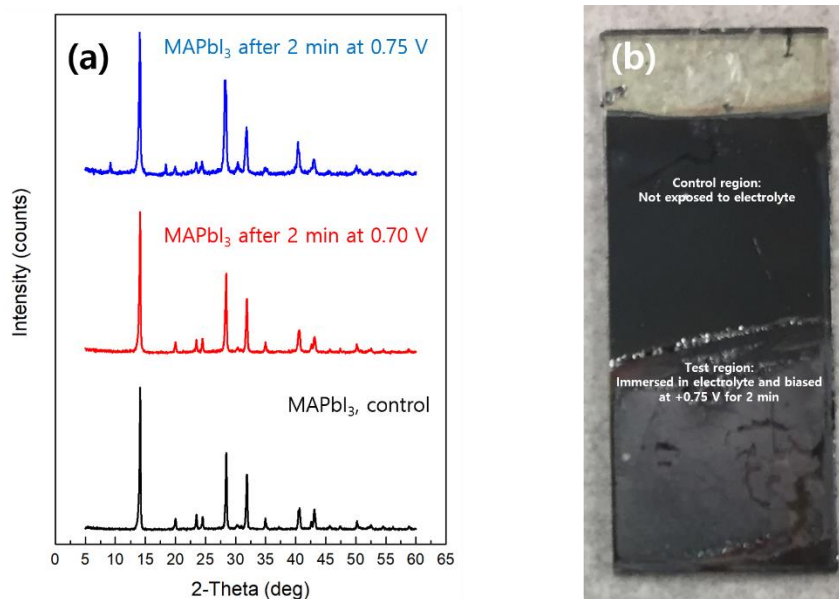


Figure 34. (a) XRD plot of MAPbI_3 perovskite films after electrochemical stability tests in 100 mM dimer electrolyte, biased at a constant potential for 2 min. (b) Photo of MAPbI_3 perovskite film after 2 min of bias at 0.75 V vs. Ag/Ag^+

To gain an idea of the identity of the unknown degradation product, further corrosion studies were performed in various electrolyte compositions. Biasing in pure DCM was performed by constant current since the absence of supporting electrolyte made controlled-potential methods impractical due to the high solution resistance. After pushing a constant current of 0.02 mA/cm^2 through the MAPbI_3 film for 2 min in DCM, XRD revealed the presence of the unknown degradation product yet again, with an identical peak position of 9.16° reappearing (Figure 35). Thus, the corrosion event between 0.70 and 0.75 V can be attributed to a material formed through either 1) interaction between DCM and perovskite, or 2) degradation events occurring internally in the perovskite film.

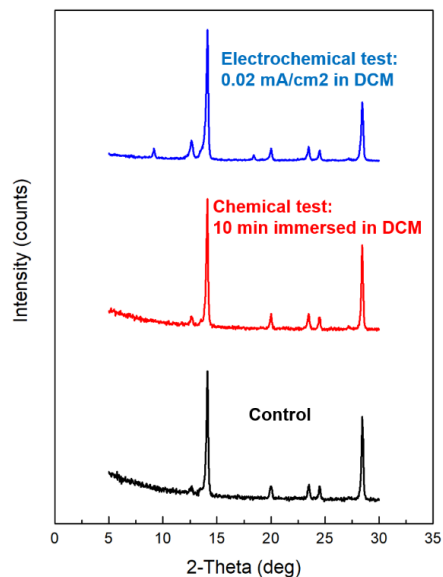


Figure 35. XRD of MAPbI_3 after chemical and electrochemical tests in DCM

3.2.4 Conclusion

Electrolytes with low polymerization potentials were developed and utilized for chemical and electrochemical compatibility tests of perovskite films. MAPbI₃ was found to be chemically stable in both dimer and trimer electrolytes, and electrochemically stable up to at least 0.70 V vs. Ag/Ag⁺ in the dimer electrolyte. At 0.75 V, MAPbI₃ degrades into an unknown degradation product. This product is a result of degradation internally in the perovskite film or interaction with the DCM solvent. At the moment, electropolymerization onto MAPbI₃ perovskite from an electrolyte containing the thiophene trimer seems to hold the most promise for in situ polythiophene deposition, as the polymerization potential for 10 mM concentration (0.75 V) lies very close to a potential that does not degrade the perovskite (0.70 V).

Chapter 4. Summary of the Thesis and Future Work

Electrodeposition of polythiophene has been demonstrated as a promising solution for industrial-scale fabrication of the HTL component in PSCs. The method utilizes cheap precursors that can be deposited with a high material utilization rate, cutting the material cost down to a fraction of that of alternative methods. Polythiophene films have been successfully synthesized by electrochemical polymerization and optimized to produce milli- and nanoscale uniform films. A 100 cm² deposition was demonstrated and proved the technique's ability to deposit highly uniform films on large substrates. The hole-transporting capabilities of the electrodeposited polythiophene was demonstrated by implementation into inverted structure solar cells, demonstrating PCEs up to 6.9%. Electrochemical stability tests have indicated that the polymerization potential of the thiophene trimer may be low enough to allow for electrodeposition onto MAPbI₃ perovskite.

For the future, the focus will be on improving the performance of the electrodeposited polythiophene in inverted structure PSCs. Surface treatments of the polythiophene films will be explored as a tool to establish conformal contact at the polythiophene/perovskite interface. Furthermore, the large-area deposited films will be incorporated into PSCs to evaluate the consistency in solar cell performance across the deposited film.

Chapter 5. Experimental Setup

5.1 Electrodes

Indium tin oxide (ITO) (130 nm thickness on 1 mm thick 2.5x2.5cm² glass substrate) was employed as the working electrode. Prior to usage, the ITO slides were sonicated for 4x15 min in Hellmanex III (2% in distilled water), distilled water, acetone, and isopropyl alcohol, and subsequently dried in a 60°C oven for ~2-3 hours. Platinum foil (25x25mm²) was employed as the counter electrode. The foil was polished with sandpaper (600 grit) and rinsed with dichloromethane before use. A non-aqueous silver/silver ion (Ag/Ag⁺) reference electrode was used as the reference electrode, with the silver wire suspended in an internal electrolyte of 0.01 M AgNO₃ and 0.1 M Bu₄NPF₆ in acetonitrile. The electrode was stored in 0.1 M Bu₄NPF₆ in acetonitrile, and quickly rinsed with acetonitrile before use.

5.2 Electrochemical Cell Setup

Two electrochemical cell designs were utilized for the electrochemical experiments, hereby referred to as simple glass cell and PTFE deposition cell.

5.2.1 Simple glass cell

For the simple glass cell, a glass vial with a screw-on lid was employed. Holes were drilled into the lid (one for each electrode) to allow for electrical connections between the potentiostat and the electrodes. The two holes for the working and the counter electrode were spaced 20 mm apart to ensure fixed

separation across all experiments. A threaded rod with an alligator clip soldered to the bottom end was inserted through each of these two holes and tightened with bolts to ensure that its position was the same for every experiment. The reference electrode was inserted through the remaining hole, where it was positioned so that the tip leaned against the edge of the working electrode. The planar working and counter electrodes were positioned parallel to one another with a separation of ~20 mm, while the reference electrode was placed next to the edge of the working electrode.

5.2.2 PTFE cell

The PTFE deposition cell was made up of two parts; a base to which the electrodes and electrolyte were added and a lid to prevent solvent evaporation and allow for performing experiments in inert atmosphere. Each part was drilled out from a single piece of PTFE. The base contained a rectangular hole of 32 mm x 6 mm area and 21.5 mm depth, with 1 mm thick walls extending up from the 32 mm sides of the hole, giving a total height of 25 mm from the bottom of the hole to the top of the wall. The WE and CE were inserted at opposite sides of the hole by using the walls for support to attach the alligator clips. By positioning the WE and CE all the way on one end of the 32 mm length, the RE could be inserted in the resulting gap on the opposite side. The cell was designed in collaboration with Dan Davies.

5.3 Electrolytes

All chemicals were stored inside an argon-filled glovebox (0.3 ppm H₂O). All electrolytes studied contained 0.1 M tetrabutylammonium hexafluorophosphate (Bu₄NPF₆) in dichloromethane (DCM) solvent. For polymerizations, the thiophene dimer (2,2'-bithiophene) or trimer (2,2':5',2''-terthiophene) was added to this solution.

5.4 Potentiostat

Electrochemical control and measurements were performed with a Bio-Logic SP-150 potentiostat.

5.5 Synthesis, Wash, and Storage of Polythiophene Films

Films were grown on an ITO working electrode. After synthesis, the films were washed by suspending them in a DCM-filled vial and shaking 5-10 sec. Films were stored in an aluminum foil-covered container inside a desiccator.

5.6 Synthesis of Thin Film Perovskites

5.6.1 CH₃NH₃PbI₃ (MAPbI₃) perovskites

0.69 g lead iodide (PbI₂) and 0.24 g methylammonium iodide (CH₃NH₃I) were dispersed in 900 μL dimethylformamide (DMF) and 100 μL dimethyl sulfoxide (DMSO), and 30 μL methylammonium in ethanol and a magnetic stir bar added. The solution was then sealed with parafilm in an airtight vial to protect from oxygen

and moisture in air, wrapped with aluminum foil to protect from incident light, and left on a hotplate at 75 °C under 350 rpm stirring for 12-18 hrs. The solution was then spin-coated on the plasma-cleaned ITO slides; 65 μ L of the $\text{CH}_3\text{NH}_3\text{PbI}_3$ solution was pipetted onto clean ITO glass (20 by 25 mm^2), spun at 2000 rpm for 25 sec, then at 3000 rpm for 7 sec, at which time 1 mL of diethyl ether anti-solvent was pipetted onto the slide. The slides were then placed on a hotplate at 100 °C for 15 min, which completes the crystallization of perovskite on ITO.

5.6.2 $\text{Cs}_{0.05}\text{FA}_{0.79}\text{MA}_{0.16}\text{Pb}(\text{Br}_{0.16}\text{I}_{0.84})_3$ (mixed-cation) perovskite

All films were prepared by Moses Kodur from the Fenning group.

5.7 Chemical and Electrochemical Stability Tests of Perovskite

Chemical stability was tested by immersing a perovskite thin film in electrolyte for 30 min, while electrochemical stability was tested by employing perovskite-coated ITO as the working electrode in the simple glass cell setup.

5.8 Scanning Electron Microscopy (SEM)

Zeiss Sigma 500 SEM was used for Scanning Electron Microscopy (SEM) imaging. All samples were coated with iridium (85 mA for 8 sec) before imaging.

5.9 Fourier-Transform Infrared (FTIR) Spectroscopy

A Fourier-Transform Infrared (FTIR) spectrometer with attenuated total reflectance (ATR) attachment (Nicolet 6700 with Smart-iTR diamond ATR crystal) was used.

5.10 X-Ray Diffraction (XRD)

XRD measurements were collected with Rigaku Smartlab XRD. Medium resolution PB/PSA template with 2-Theta scan-axis was used for all samples. Scans were run at a scan speed of 1.5°/min and a step size of 0.04°.

5.11 Ultraviolet – Visible (UV-Vis) Spectroscopy

UV-Vis spectra were collected with a Perkin Elmer UV-Vis-NIR Spectrometer with the 150 mm InGaAs integrating sphere attachment. The wavelength resolution was 2 nm. The InGaAs detector was used with a gain of 9.00 and a response time of 0.24 s.

5.12 Steady-state Photoluminescence (ss-PL)

Steady-state Photoluminescence measurements were taken with a Renishaw InVia Raman Microscope.

5.13 Solar Simulator

Solar cell JV curves were collected with a 1366 Technologies solar simulator.

Bibliography

- 1) Correa-Baena, J. P., Abate, A., Saliba, M., Tress, W., Jacobsson, T. J., Grätzel, M., & Hagfeldt, A. (2017). The rapid evolution of highly efficient perovskite solar cells. *Energy & Environmental Science*, 10(3), 710-727.
- 2) Chang, N. L., Yi Ho-Baillie, A. W., Basore, P. A., Young, T. L., Evans, R., & Egan, R. J. (2017). A manufacturing cost estimation method with uncertainty analysis and its application to perovskite on glass photovoltaic modules. *Progress in Photovoltaics: Research and Applications*, 25(5), 390-405.
- 3) Sahu, N., Parija, B., & Panigrahi, S. (2009). Fundamental understanding and modeling of spin coating process: A review. *Indian Journal of Physics*, 83(4), 493-502.
- 4) Grätzel, M. (2017). Molecular photovoltaics and perovskite solar cells [Youtube video]. Retrieved from <https://www.youtube.com/watch?v=sNIReli99nU>
- 5) Jung, E. H., Jeon, N. J., Park, E. Y., Moon, C. S., Shin, T. J., Yang, T. Y., Noh, J. H., & Seo, J. (2019). Efficient, stable and scalable perovskite solar cells using poly (3-hexylthiophene). *Nature*, 567(7749), 511.
- 6) Kegelman, L., Tockhtorn, P., Wolff, C. M., Márquez, J. A., Caicedo-Dávila, S., Korte, L., Unold, T., Lövenich, W., Neher, D., Rech, B., & Albrecht, S. (2019). Mixtures of Dopant-Free Spiro-OMeTAD and Water-Free PEDOT as a Passivating Hole Contact in Perovskite Solar Cells. *ACS applied materials & interfaces*, 11(9), 9172-9181.
- 7) Yan, W., Li, Y., Sun, W., Peng, H., Ye, S., Liu, Z., & Huang, C. (2014). High-performance hybrid perovskite solar cells with polythiophene as hole-transporting layer via electrochemical polymerization. *Rsc Advances*, 4(62), 33039-33046.
- 8) Kampmann, A., Sittinger, V., Rechid, J., & Reineke-Koch, R. (2000). Large area electrodeposition of Cu(In,Ga)Se₂. *Thin Solid Films*, 361, 309-313.
- 9) Krische, B., & Zagorska, M. (1989). Polythiophene synthesis by electropolymerization of thiophene and bithiophene. *Synthetic metals*, 33(3), 257-267.
- 10) Cosnier, S., & Karyakin, A. (Eds.). (2011). *Electropolymerization: concepts, materials and applications*. John Wiley & Sons.

- 11) McCullough, R. D. (1998). The chemistry of conducting polythiophenes. *Advanced Materials*, 10(2), 93-116.
- 12) Kaneto, K., Kohno, Y., & Yoshino, K. (1984). Absorption spectra induced by photoexcitation and electrochemical doping in polythiophene. *Solid state communications*, 51(5), 267-269.
- 13) Wei, Y., Chan, C. C., Tian, J., Jang, G. W., & Hsueh, K. F. (1991). Electrochemical polymerization of thiophenes in the presence of bithiophene or terthiophene: kinetics and mechanism of the polymerization. *Chemistry of Materials*, 3(5), 888-897.
- 14) Jin, S., Cong, S., Xue, G., Xiong, H., Mansdorf, B., & Cheng, S. Z. (2002). Anisotropic polythiophene films with high conductivity and good mechanical properties via a new electrochemical synthesis. *Advanced Materials*, 14(20), 1492-1496.
- 15) Del Valle, M. A., Cury, P., & Schrebler, R. (2002). Solvent effect on the nucleation and growth mechanisms of poly (thiophene). *Electrochimica acta*, 48(4), 397-405.
- 16) Te Nijenhuis, K. (1997). Thermoreversible networks: viscoelastic properties and structure of gels (Vol. 130, pp. 37-66). Berlin Heidelberg: Springer.
- 17) Yan, W., Li, Y., Li, Y., Ye, S., Liu, Z., Wang, S., Bian, Z., & Huang, C. (2015). Stable high-performance hybrid perovskite solar cells with ultrathin polythiophene as hole-transporting layer. *Nano Research*, 8(8), 2474-2480.
- 18) Aeiyaich, S., Bazzaoui, E. A., & Lacaze, P. C. (1997). Electropolymerization of thiophene on oxidizable metals in organic media. *Journal of Electroanalytical Chemistry*, 434(1-2), 153-162.
- 19) Krische, B., & Zagorska, M. (1989). The polythiophene paradox. *Synthetic Metals*, 28(1-2), 263-268.
- 20) Camarada, M. B., Jaque, P., Díaz, F. R., & Del Valle, M. A. (2011). Oxidation potential of thiophene oligomers: theoretical and experimental approach. *Journal of Polymer Science Part B: Polymer Physics*, 49(24), 1723-1733.
- 21) Nicolau, Y. F., & Moser, P. (1993). Study of free volume and crystallinity in polybithiophene and poly (3-methylthiophene). *Journal of Polymer Science Part B: Polymer Physics*, 31(11), 1529-1543.

- 22) Bard, A. J., Faulkner, L. R., Leddy, J., & Zoski, C. G. (1980). *Electrochemical methods: fundamentals and applications* (Vol. 2). New York: Wiley.
- 23) Noel, N. K., Abate, A., Stranks, S. D., Parrott, E. S., Burlakov, V. M., Goriely, A., & Snaith, H. J. (2014). Enhanced photoluminescence and solar cell performance via Lewis base passivation of organic–inorganic lead halide perovskites. *ACS nano*, 8(10), 9815-9821.
- 24) Sherkar, T. S., Momblona, C., Gil-Escrig, L., Ávila, J., Sessolo, M., Bolink, H. J., & Koster, L. J. A. (2017). Recombination in perovskite solar cells: significance of grain boundaries, interface traps, and defect ions. *ACS energy letters*, 2(5), 1214-1222.
- 25) Yang, S., Dai, J., Yu, Z., Shao, Y., Zhou, Y., Xiao, X., Zeng, X. C., & Huang, J. (2019). Tailoring Passivation Molecular Structures for Extremely Small Open-Circuit Voltage Loss in Perovskite Solar Cells. *Journal of the American Chemical Society*, 141(14), 5781-5787.
- 26) Jiang, Q., Zhao, Y., Zhang, X., Yang, X., Chen, Y., Chu, Z., Ye, Q., Li, X., Yin, Z., & You, J. (2019). Surface passivation of perovskite film for efficient solar cells. *Nature Photonics*, 1.
- 27) Liu, X., Rezaee, E., Shan, H., Xu, J., Zhang, Y., Feng, Y., Dai, J., Chen, Z. K., Huang, W., & Xu, Z. X. (2018). Dopant-free hole transport materials based on alkyl-substituted indacenodithiophene for planar perovskite solar cells. *Journal of Materials Chemistry C*, 6(17), 4706-4713.
- 28) Nie, W., Tsai, H., Asadpour, R., Blancon, J. C., Neukirch, A. J., Gupta, G., Crochet, J., Chhowalla, M., Tretiak, S., Alam, M., Wang, H. L., & Wang, H. L. (2015). High-efficiency solution-processed perovskite solar cells with millimeter-scale grains. *Science*, 347(6221), 522-525.
- 29) Woodhouse, M. A., Smith, B., Ramdas, A., & Margolis, R. M. (2019). *Crystalline Silicon Photovoltaic Module Manufacturing Costs and Sustainable Pricing: 1H 2018 Benchmark and Cost Reduction Road Map* (No. NREL/TP-6A20-72134). National Renewable Energy Lab.(NREL), Golden, CO (United States).
- 30) Chang, N. L., Yi Ho-Baillie, A. W., Basore, P. A., Young, T. L., Evans, R., & Egan, R. J. (2017). A manufacturing cost estimation method with uncertainty analysis and its application to perovskite on glass photovoltaic modules. *Progress in Photovoltaics: Research and Applications*, 25(5), 390-405.
- 31) www.alibaba.com. (2019). Cs150 Professional Electrochemical Workstation /potentiostat /galvanostat For Corrosion/battery Test Electrochemistry Analyzer

- Buy Cs150 Professional Electrochemical Workstation /potentiostat /galvanostat For Corrosion/battery Test,Potentiostat /galvanostat For Corrosion/battery Test,Electrochemical Workstation Potentiostat Product on Alibaba.com. [online] Available at: https://www.alibaba.com/product-detail/CS150-professional-Electrochemical-Workstation-Potentiostat-Galvanostat_60456430855.html?spm=a2700.7724838.0.0.7b153aa89hgWOr [Accessed 9 Dec. 2019].

- 32) Song, Z., McElvany, C. L., Phillips, A. B., Celik, I., Krantz, P. W., Wathage, S. C., Liyanage, G. K., Apul, D., & Heben, M. J. (2017). A technoeconomic analysis of perovskite solar module manufacturing with low-cost materials and techniques. *Energy & Environmental Science*, 10(6), 1297-1305.
- 33) San Diego, CA Electricity Rates. (n.d.). Retrieved from <https://www.electricitylocal.com/states/california/san-diego/#:~:targetText=The average residential electricity rate in San Diego is 16.35,rate of 11.88¢/kWh>.
- 34) Jones-Albertus, R., Feldman, D., Fu, R., Horowitz, K., & Woodhouse, M. (2016). Technology advances needed for photovoltaics to achieve widespread grid price parity. *Progress in photovoltaics: research and applications*, 24(9), 1272-1283.
- 35) Meng, X., Bai, Y., Xiao, S., Zhang, T., Hu, C., Yang, Y., Zheng, X., & Yang, S. (2016). Designing new fullerene derivatives as electron transporting materials for efficient perovskite solar cells with improved moisture resistance. *Nano Energy*, 30, 341-346.
- 36) Zhao, D., Zhu, Z., Kuo, M. Y., Chueh, C. C., & Jen, A. K. Y. (2016). Hexazatrinaphthylene Derivatives: Efficient Electron-Transporting Materials with Tunable Energy Levels for Inverted Perovskite Solar Cells. *Angewandte Chemie International Edition*, 55(31), 8999-9003.
- 37) Samu, G. F., Scheidt, R. A., Zaiats, G., Kamat, P. V., & Janáky, C. (2018). Electrodeposition of Hole-Transport Layer on Methylammonium Lead Iodide Film: A Strategy To Assemble Perovskite Solar Cells. *Chemistry of Materials*, 30(13), 4202-4206.
- 38) Samu, G. F., Scheidt, R. A., Kamat, P. V., & Janáky, C. (2017). Electrochemistry and spectroelectrochemistry of lead halide perovskite films: materials science aspects and boundary conditions. *Chemistry of Materials*, 30(3), 561-569.

- 39) Xie, F., Chen, C. C., Wu, Y., Li, X., Cai, M., Liu, X., Yang, X., & Han, L. (2017). Vertical recrystallization for highly efficient and stable formamidinium-based inverted-structure perovskite solar cells. *Energy & Environmental Science*, 10(9), 1942-1949.